Journal of Medicinal Chemistry

Article

Discovery of a Non-Covalent, Mutant-Selective Epidermal Growth Factor Receptor Inhibitor

Bryan K Chan, Emily J. Hanan, Krista Bowman, Marian C. Bryan, Daniel J. Burdick, Emily W. Chan, Yuan Chen, Saundra Clausen, Trisha Dela Vega, Jennafer Dotson, Charles Eigenbrot, Richard L Elliott, Robert Andrew Heald, Philip S Jackson, Jamie D Knight, Hank La, Michael David Lainchbury, Shiva Malek, Hans E. Purkey, Gabriele Schaefer, Stephen Schmidt, Eileen M Seward, Steve Sideris, Lily Shao, Shumei Wang, Kuen S Yeap, Ivana Yen, Christine Yu, and Timothy P Heffron

J. Med. Chem., **Just Accepted Manuscript** • DOI: 10.1021/acs.jmedchem.6b00995 • Publication Date (Web): 26 Aug 2016

Just Accepted

ACS Publications

Journal of Medicinal Chemistry is published by the American Chemical Society. 1155 Sixteenth Street N.W., Washington, DC 20036

Discovery of a Non-Covalent, Mutant-Selective Epidermal Growth Factor Receptor Inhibitor

Bryan K. Chan,[*,†] *Emily J. Hanan,*[†] *Krista K. Bowman,*[⊥] *Marian C. Bryan,*[†] *Daniel Burdick,*[†] *Emily Chan,*[□] *Yuan Chen,*[§] *Saundra Clausen,*[◊] *Trisha Dela Vega,*[⊥] *Jennafer Dotson,*[†] *Charles Eigenbrot,*[‡] *Richard L. Elliott,*[Δ] *Robert A. Heald,*[Δ] *Philip S. Jackson,*[Δ] *Jamie D. Knight,*[Δ] *Hank La,*[§] *Michael D. Lainchbury,*[Δ] *Shiva Malek,*[◊] *Hans Purkey,*[†] *Gabriele Schaefer,*[#] *Stephen Schmidt,*[◊] *Eileen M. Seward,*[Δ] *Steve Sideris,*[◊] *Lily Shao,*[□] *Shumei Wang,*[†] *Kuen S. Yeap,*[Δ] *Ivana Yen,*[◊] *Christine Yu,*[‡] *Timothy P. Heffron*[†]

[†]Departments of Discovery Chemistry, [‡]Structural Biology, [§]Drug Metabolism and Pharmacokinetics, [◊]Biochemical and Cellular Pharmacology, [#]Molecular Oncology, [□]Research Oncology and [⊥]Protein Expression Genentech Inc., 1 DNA Way, South San Francisco, California, 94080, United States. [Δ] Discovery, Charles River, 7/9 Spire Green Centre, Flex Meadow, Harlow, Essex CM19 5TR, United Kingdom.

KEYWORDS

Kinase, kinase inhibitor, EGFR, T790M, resistance mutant, structure-based drug design

Abstract

Inhibitors targeting the activating mutants of the epidermal growth factor receptor (EGFR) have found success in the treatment of EGFR-mutant positive non-small cell lung cancer. A secondary point mutation (T790M) in the inhibitor binding site has been linked to the acquired resistance against those first generation therapeutics. Herein, we describe the lead optimization of a series of reversible, pan-mutant (L858R, $del_{746-750,}$ T790M/L858R and T790M/$del_{746-750}$) EGFR inhibitors. Using a non-covalent double mutant (T790M/L858R and T790M/$del_{746-750}$) selective EGFR inhibitor (**2**) as a starting point, activities against the single mutants (L858R and $del_{746-750}$) were introduced through a series of structure-guided modifications. The in vitro ADME-PK properties of the lead molecules were further optimized through a number of rational structural changes. The resulting inhibitor (**21**) exhibited excellent cellular activity against both the single and double mutants of EGFR, demonstrated target engagement in vivo and ADME-PK properties that are suitable for further evaluation. The reversible, non-covalent inhibitors described complement the covalent pan-mutant EGFR inhibitors that have shown encouraging results in recent clinical trials.

Introduction

The role of activating mutants of the epidermal growth factor receptor (EGFR) in non-small cell lung cancer (NSCLC) is well-documented.[1-5] The most common activating mutants, the point mutation L858R or deletions within exon 19 ($del_{746-750}$), increase EGFR-driven cell proliferation and survival. The first generation EGFR inhibitors (erlotinib and gefitinib) that target those activating mutants have demonstrated a remarkable initial rate of clinical response in the treatment of EGFR-mutated NSCLC.[6-10] Additionally, a number of second-generation EGFR

inhibitors that covalently target the Cys797 residue within the EGFR ATP binding site have been reported.[11-12] While both first and second generation EGFR inhibitors demonstrated clinical efficacy, this efficacy is accompanied by skin and gastrointestinal toxicities that are believed to be associated with their inhibitory activity towards the wild type form of EGFR (wtEGFR).

In addition, acquired resistance against these therapeutic agents follows.[12-16] Approximately 60% of the acquired resistance arises from a secondary point mutation of the gatekeeper residue Thr790 to methionine (T790M) within the EGFR kinase domain.[17-19] This mutation, while maintaining catalytic function of the enzyme, reduces the inhibitory effect of erlotinib and gefitinib by occluding part of the binding site for these molecules while simultaneously increasing the kinase's affinity for ATP.[20-24]

Recently, promising clinical results have been reported for the third generation inhibitors (osimertinib and rociletinib) that were designed to covalently inhibit both the activating mutations and the T790M resistance mutation while sparing wtEGFR.[16,25-30] These results have led to the FDA approval of osimertinib for the treatment of patients with metastatic EGFR T790M-positive NSCLC who have progressed on or after other EGFR-blocking therapies. Despite this remarkable advance, clinical cases of the Cys797 to serine point mutation (C797S) conferring resistance to covalent inhibitors by eliminating the point of covalent modification have recently been reported.[16,31-33] Anticipating such a resistance mechanism, it was our goal to identify a non-covalent, mutant selective EGFR inhibitor.

We previously reported a series of potent and selective inhibitors of the resistance mutants of EGFR (**1** and **2,** Table 1).[34,35] Aminopyrimidine inhibitors **1** and **2** demonstrated excellent biochemical potency against the T790M-L858R (TMLR) and T790M-del$_{746\text{-}750}$ (TMdel) resistance double mutants of EGFR. These molecules inhibit the T790M mutants with high

selectivity over wtEGFR, which was appealing for safety considerations. However, **1** and **2** each lack biochemical inhibitory effects on the initial T790-containing single activating mutants of EGFR (L858R and $del_{746-750}$). A similar T790M selectivity profile of **1** and **2** was also observed in cellular EGFR autophosphorylation (pEGFR) assays, comparing activity in the TMLR expressing (H1975) and TMdel expressing (PC9-ER) cell lines against activity in the $del_{746-750}$ expressing (PC9) and wtEGFR (H292) cell lines.

As reports indicate the importance of sustained inhibition of EGFR activating mutants beyond initial progression on first generation EGFR inhibitor therapy, we sought to improve upon **1** and **2** by incorporating inhibition of the activating single mutants of EGFR along with the T790M double mutants.[36] Given their attractive overall physicochemical profiles, high selectivity against wtEGFR and our knowledge of their structure-activity relationships, the aminopyrimidine inhibitors (**1** and **2**) were chosen as the starting points towards a non-covalent, wtEGFR-sparing, pan-mutant EFGR inhibitor.

Table 1. Reversible T790M resistance mutant-selective inhibitors.

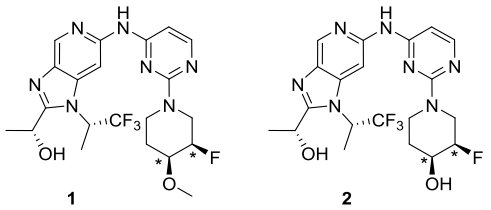

Cmpd	TMLR Ki_{app} (nM)[c]	TMdel Ki_{app} (nM)[c]	L858R Ki_{app} (nM)[c]	$del_{746-750}$ Ki_{app} (nM)[c]	wtEGFR Ki_{app} (nM)[c]	pEGFR H1975 IC_{50} (μM)[d]	pEGFR PC9-ER IC_{50} (μM)[d]	pEGFR PC9 IC_{50} (μM)[d]	pEGFR H292 IC_{50} (μM)[d]
1[a]	1.1	7.0	77	490	122	0.021	0.027	2.6	>10
2[b]	2.5	6.0	223	572	313	0.261	0.081	5.4	>10

[a]Compound **1** was a 1:1 mixture of (*R*)-1-(6-((2-((3*R*,4*S*)-3-fluoro-4-methoxypiperidin-1-yl)pyrimidin-4-yl)amino)-1-((*S*)-1,1,1-trifluoropropan-2-yl)-1*H*-imidazo[4,5-*c*]pyridin-2-yl)ethan-1-ol and (*R*)-1-(6-((2-((3*S*,4*R*)-3-fluoro-4-methoxypiperidin-1-yl)pyrimidin-4-yl)amino)-1-((*S*)-1,1,1-trifluoropropan-2-yl)-1*H*-imidazo[4,5-*c*]pyridin-2-yl)ethan-1-ol.[34] [b]Compound **2** was a 1:1 mixture of (3*R*,4*S*)-3-fluoro-1-(4-((2-((*R*)-1-hydroxyethyl)-1-((*S*)-1,1,1-trifluoropropan-2-yl)-1*H*-imidazo[4,5-*c*]pyridin-6-yl)amino)pyrimidin-2-yl)piperidin-4-ol and (3*S*,4*R*)-3-fluoro-1-(4-((2-((*R*)-1-hydroxyethyl)-1-((*S*)-1,1,1-trifluoropropan-2-yl)-1*H*-imidazo[4,5-*c*]pyridin-6-yl)amino)pyrimidin-2-yl)piperidin-4-ol.[34] [c]Biochemical assays. All Ki data measurements reported are the geometric means of at least two independent experiments. [d]Inhibition of EGFR auto-phosphorylation. All IC_{50} data measurements reported are the geometric means of at least two independent experiments. H1975: Double mutant TMLR cell line. PC9-ER: Double mutant TMdel cell line. PC9: Activating mutant $del_{746\text{-}750}$ EGFR cell line. H292: wild type EGFR cell line.

Results and Discussions

As previously described, the selectivity of **1** and **2** for the T790M mutants over wtEGFR and the activating mutants was attributed to the favorable hydrophobic interactions between the 4-alkoxypiperidine group and the side chain of the methionine gatekeeper (Figure 1B).[34] Fluorine substitution at the 3-position of the piperidine further enhanced those favorable interactions and resulted in enhanced inhibition of the T790M mutants, while sparing the activating single mutants. The 4-hydroxyl or 4-alkyoxy substitutions of the piperidine group were critical to potency as they form a hydrogen bonding interaction with the conserved, catalytic Lys745. In order to generate an inhibitor that exhibits activities against the T790M resistance double mutants as well as the activating single mutants of EGFR, we hypothesized that it would be necessary to identify a replacement for the T790M-selective piperidine motif.

Through a library approach, a number of aliphatic amines were examined and found to be inadequate replacements for the piperidine group.[34] Significant loss of potency was typically observed. In parallel, we embarked on a structure-based design approach with the aim of identifying a replacement for the 4-alkoxypiperidine group that could engage Lys745 and the P-loop residue Phe723. Since those two residues are conserved among all EGFR forms, we

hypothesized that engaging those residues could result in favorable binding interactions toward both T790- and T790M-carrying mutants.

Figure 1. (A) T790M selective inhibitor **3**. Absolute stereochemistry of all asymmetric centers is as shown. (B) Overlay of a model of *N*-alkylsulfonylpyrazole design (green) with x-ray structure of resistance mutant-selective inhibitor **3** complexed with EGFR TMLR double mutant (ligand: orange; protein: cyan; PDB code 5CAS). Predicted hydrogen bond interactions are shown as yellow dashed lines.

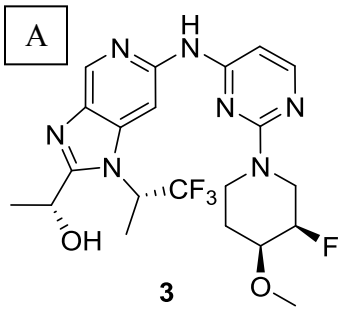

TMLR Ki = 2 nM
wtEGFR Ki = 180 nM

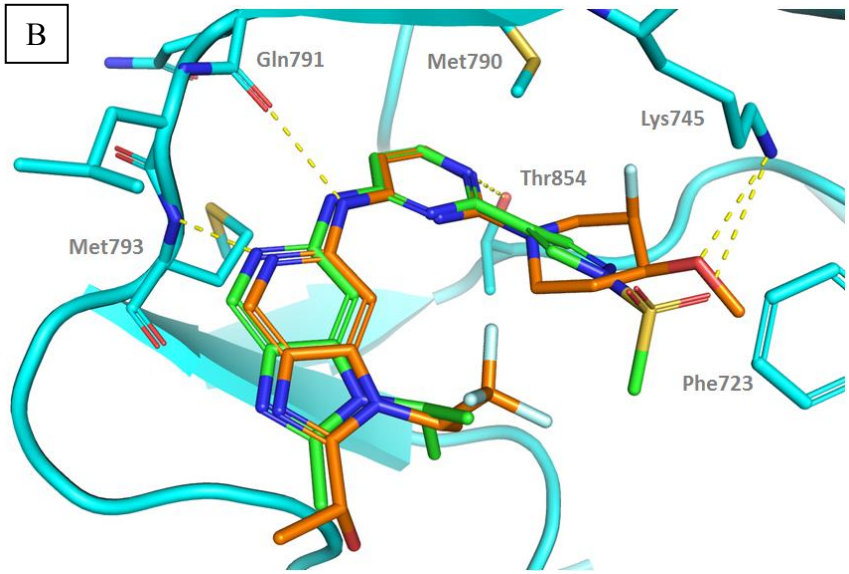

An examination of the x-ray structure of a representative T790M selective inhibitor (**3**, Figure 1A) in the TMLR double mutant form of EGFR suggested that it would be desirable to position a hydrogen bond acceptor approximately five bond lengths distal from the pyrimidine ring in order to engage Lys745 (Figure 1B). A number of aliphatic systems that satisfied this requirement were tested and yielded disappointing results.[34] Further modeling results suggested that an *N*-alkylsulfonylpyrazole would position a hydrogen bond acceptor, namely the sulfonyl oxygen, within hydrogen bonding distance from the ammonium group of Lys745 (Figure 1B). Furthermore, the terminal alkyl group would also be within the appropriate distance to engage the side chain of Phe723 via hydrophobic interactions.

To test the hypothesis, compound **6** was synthesized using the simplified achiral azabenzimidazole moiety as a model system for synthetic ease (Table 2). Compound **6** demonstrated either comparable or improved activity against the TMLR double mutant and TMdel double mutants of EFGR when compared to the previously optimized piperidine-based inhibitors **4** and **5** (Table 2). Gratifyingly, compound **6** also showed improved potency against the L858R and $del_{746\text{-}750}$ single activating mutants. Expansion of the methylsulfonyl group to a cyclopropylsulfonyl group (**7**) further improved potency for all forms of EGFR. The increase in activity for the bulkier cyclopropyl analog could possibly be due to the increase in hydrophobic interactions or, more specifically, π-interactions between the partially sp^2-hybridized cyclopropyl group and the π-face of the aromatic side chain of Phe723. The cyclopropylmethyl analog **8** showed reduced inhibitory activity against the TMLR double mutant, which we attribute to its inability to engage Lys745 in a hydrogen bonding interaction (the other mutant forms were not tested).

Table 2. Piperidine Replacements.

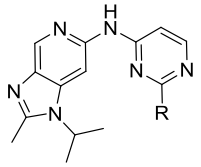

Cmpd	R	TMLR Ki_{app} (nM)[a]	TMdel Ki_{app} (nM)[a]	L858R Ki_{app} (nM)[a]	$del_{746-750}$ Ki_{app} (nM)[a]	wtEGFR Ki_{app} (nM)[a]
4[b]	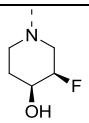	13	43	1100	1300	905
5	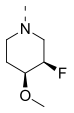	3.6	41	608	1800	896
6	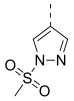	18	3.5	126	38	324
7	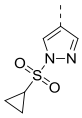	4.1	1.8	43	12	55
8		34	-	-	-	1200

[a]Biochemical assays. All Ki data measurements reported are the geometric means of at least two independent experiments. [b]Racemic; Relative stereochemistry as shown.

Figure 2. X-ray structure of **7** complexed with EGFR TMLR double mutant (PDB code 5HCX). Predicted hydrogen bond interactions are shown as yellow dashed lines. Interatom distance is indicated by dashed purple lines with values in Å.

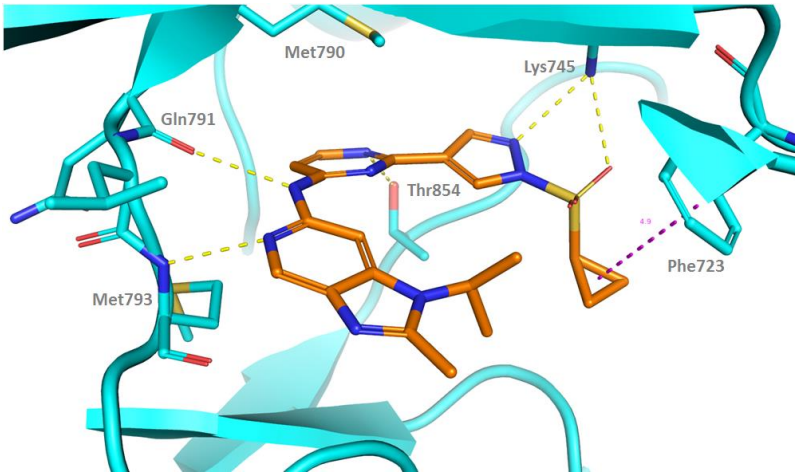

An x-ray structure of **7** in the TMLR double mutant was obtained to confirm the binding mode of the inhibitor (Figure 2). In line with the previously disclosed structures of the inhibitors within this series, the amino-azabenzimidazole forms two hydrogen bonds with the backbone of Gln791 and Met793 in the hinge region of the binding site.[34,35] The pyrimidyl group of the inhibitor is positioned under the Met790 gatekeeper side chain and engages Thr854 via hydrogen bonding. The *N*-cyclopropylsulfonyl-pyrazole appears to engage the ammonium group of Lys745 via both the sulfonyl oxygen (3.0 Å) and the pyrazole nitrogen (3.0 Å). The cyclopropylsulfonyl motif is also situated to engage the phenyl side chain of Phe723 via hydrophobic interactions.

Table 3. In vitro ADME data for **4** and **7**.

Cmpd	Liver microsome Cl_{hep} H/R/M (ml $min^{-1}kg^{-1}$)[a]	Hepatocyte Cl_{hep} H/R/M (ml $min^{-1}kg^{-1}$)[b]	MDCK P_{app} A-B (x 10^{-6} cm s^{-1})[c]
4	5.2/12/76	9.0/11/69	19
7	7.7/20/70	4.0/17/49	21

[a]H/R/M = human/rat/mouse. [b]in vitro stability in cryopreserved hepatocytes. [c]A-B, apical-to-basolateral. See experimental section for details of assay errors and controls.

Compound **7** demonstrated comparable in vitro metabolic stability and permeability properties to the corresponding hydroxypiperidine analog **4** (Table 3). Most importantly, both **4** and **7** had acceptable predicted human clearance as extrapolated from in vitro liver microsome and hepatocyte data. Because of its promising overall profile, the *N*-cyclopropylsulfonyl-pyrazole group was used in subsequent optimization of the other parts of the molecule with the goal of further improving potency while maintaining acceptable ADME attributes.

The vector extending from the 3-position of the azabenzimidazole system had been underexplored to this point (Table 4). To access this vector, replacement of the azabenzimidazole group with bioisosteric systems such as an azaindazole or azaindole would be required. Optimization on an azaindole system was first explored as it was previously found to have potency comparable to that of the azabenzimidazole.[35] Due to the high lipophilicity of the scaffold in general (cLogP of **7** = 3.6) and a desire to reduce the metabolic liability of an electron-rich azaindole heterocycle, we first focused on polar electron-withdrawing substituents such as carboxamides.

Table 4. Azaindole-3-carboxamide and azaindazole-3-carboxamide SAR.

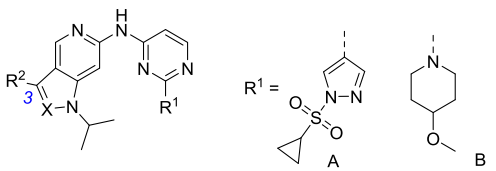

Cmpd	X	R^1	R^2	TMLR Ki_{app} (nM)[a]	TMdel Ki_{app} (nM)[a]	L858R Ki_{app} (nM)[a]	$del_{746\text{-}750}$ Ki_{app} (nM)[a]	wtEGFR Ki_{app} (nM)[a]	MDCK A-B P_{app} (10^{-6} cms^{-1})[b]	K. Sol (μM)[c]

9	CH	A	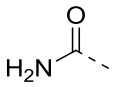	1.1	0.35	4.1	1.2	7.8	4.5	<1
10	CH	B	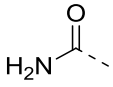	5.3	27	363	323	167	26	3
11	N	B	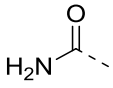	29	-	-	-	>1000	-	-
12	CH	A	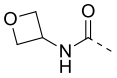	1.1	2.0	6.4	2.0	4.6	2.3	7
13	CH	A	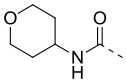	1.2	1.6	3.8	1.4	3.4	4.6	11

[a]Biochemical assays. All Ki data measurements reported are the geometric means of at least two independent experiments. [b]A-B, apical-to-basolateral. [c]Aqueous kinetic solubility at pH 7.4.

Gratifyingly, the 3-carboxamide azaindole **9** resulted in improved potency compared to azabenzimidazole **7** for both the T790- and T790M-carrying mutants of EGFR (Table 4). The gain in potency could possibly be attributed to water-mediated hydrogen bonding interactions between the carboxamide and the backbone carbonyl of Pro794 (Figure **3A**). In the context of the 4-methoxypiperidine group (**10**), we again observed reduced potency for the L858R and $del_{746\text{-}750}$ single mutants relative to the T790M double mutants, suggesting that the 3-carboxamide group did not alter the mutant-selectivity of the inhibitor.

Modest permeability was observed for **9**, possibly due to its high TPSA (150 $Å^2$). Reducing the number of hydrogen bond donors in a molecule is a well-established strategy to improve permeability.[37] We envisioned that conversion of the azaindole to an azaindazole could mask the NH functionality of the amide via an intramolecular hydrogen bond, and therefore improve permeability. The 3-amido-azaindazole **11**, however, showed a significant loss of potency. With the increase in polarity, the azaindazole may have reduced favorable, hydrophobic contacts with the surrounding lipophilic residues (*vide supra*).

Alternatively, the primary amide was replaced with a variety of the secondary amides to reduce the hydrogen bond donor count and improve aqueous solubility by deterring intermolecular hydrogen bonding (e.g. dimerization). Indeed, the oxetanyl (**12**) and tetrahydropyranyl (**13**) carboxamides demonstrated improved aqueous solubility. However, permeability remained modest. Possibly due to the combination of modest solubility and permeability, after a single oral dose of 100 mg/kg (MCT suspension) in mouse, plasma concentration of **13** was below the lowest level of quantification. The 3-carboxamide series was thus deprioritized. Nonetheless, the 3-amido-azaindole analogs demonstrated that significant potency gain can be achieved by substituting at the 3-position of the [6,5]-bicyclic scaffold.

Figure 3. (A) X-ray structure of **13** in EGFR TMLR double mutant (PDB code 5HCY). Predicted hydrogen bond interactions are shown as yellow dashed lines (B) X-ray structure of **13** in EGFR TMLR double mutant with interaction surface shown. Color of surface indicates element (pink = oxygen; cyan = nitrogen; gray = carbon).

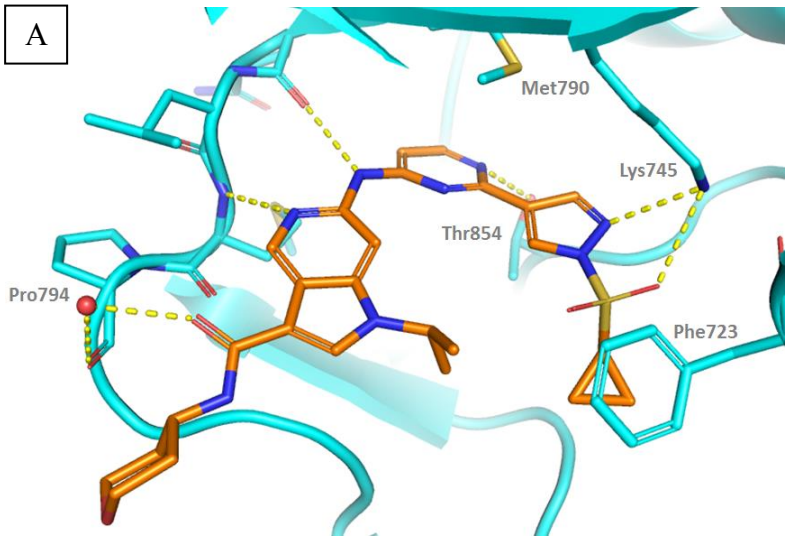

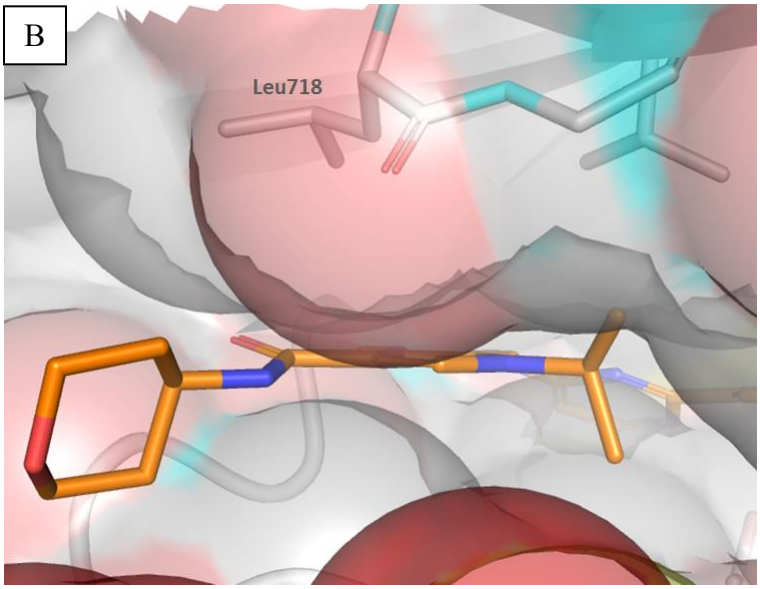

Close examination of the x-ray structure of **13** suggested that the C3-vector of the azaindole is situated under the lipophilic chain side of Leu718 in a narrow channel and 3-dimensional steric bulk should only be tolerated beyond approximately two bond lengths from the azaindole core structure (Figure 3B). To optimally occupy this space, a substitution would need to be lipophilic and structurally planar proximal to the [6,5]-bicyclic scaffold. Despite their apparent fit to this pocket, aryl motifs were considered to be undesirable due to their propensity to negatively impact aqueous solubility.[38] We hypothesized that a dialkylamino motif should satisfy the requirements. To prevent further elevation of lipophilicity, heteroatoms were incorporated into the C3-substituents.

Table 5. 3-Amino-azaindazole SAR.

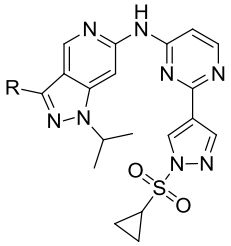

Cmpd	R	TMLR Ki_{app} (nM)[a]	wtEGFR Ki_{app} (nM)[a]	p-EGFR H1975 IC_{50} (μM)[b]	p-EGFR PC9-ER IC_{50} (μM)[b]	p-EGFR PC9 IC_{50} (μM)[b]	p-EGFR H292 IC_{50} (μM)[b]	CL HLM[c]/ CL HHep[d] (ml min^{-1} kg^{-1})	MDCK A-B P_{app} (x 10^{-6} cm s^{-1})[e]	Kin Sol. (μM)[f]
14		0.79	8.2	0.064	0.014	0.080	3.9	13/8.4	16	2
15		2.1	10	0.074	0.019	0.076	0.85	9.3/6.7	12	1
16	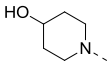	1.2	5.5	0.092	0.015	0.046	1.5	7.0/7.7	12	1
17	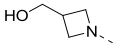	<0.6	2.0	0.019	0.0081	0.028	0.096	10/13	8.1	3
18	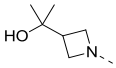	<0.6	7.0	0.032	0.010	0.13	0.21	8.9/7.1	20	<1
19		24	>531	2.4	0.91	3.0	>10	8.5/15	3.9	<1

[a]Biochemical assays. All Ki data measurements reported are the geometric means of at least two independent experiments. [b]Inhibition of EGFR auto-phosphorylation. All IC_{50} data measurements reported are the geometric means of at least two independent experiments. H1975: Double mutant TMLR EGFR cell line. PC9-ER: Double mutant TMdel EGFR cell line. PC9: Activating mutant $del_{746\text{-}750}$ EGFR cell line. H292: Wild type EGFR cell line. [c]Metabolic clearance from human liver microsomes. [d]Metabolic clearance from cryopreserved human hepatocytes. [e]A-B, apical-to-basolateral. [f]Kinetic solubility at pH 7.4.

Although the azaindole system had demonstrated excellent potency, we opted to focus on azaindazoles to study the C3-amine substitution to avoid the presence of a highly electron-rich 3-amino-azaindole system that could be a metabolic liability. In addition, given the excellent biochemical potency of the C3-substituted azaindole or azaindazole inhibitors, we opted to evaluate the potency of the compounds through the use of the cellular autophosphorylation assays (Table 5).

We previously found that 3-amino-azaindazoles had good activity against the TMLR double mutant, and that finding was recapitulated in the context of the *N*-cyclopropylsulfonyl-pyrazole (**14**).[35] Expansion of the amino group to the morpholine (**15**) maintained cellular potency for

both the activating $del_{746\text{-}750}$ mutant (PC9) and T790M double mutant (H1975 and PC9-ER) cell lines. The 4-hydroxypiperidine analog **16** was also tolerated by all mutant forms, while the hydroxymethylazetidine analog **17** provided improved potency. Introduction of the *gem*-dimethyl substitution (**18**) to sterically mask the hydrogen bond donor improved permeability. The tertiary alcohol **18** also showed improved hepatocyte stability relative to primary alcohol **17**. As predicted, replacement of the dialkylamino motif with a 3-dimensional alkyl group (**19**) resulted in considerable loss in activity. At this point, compound **18** was chosen for further optimization due to its balanced pharmacological and ADME profiles.

From our previous work on the azabenzimidazole series, we learned that further potency gains could be realized by expanding the *N1*-alkyl substitution of the azabenzimidazole system, given that it is a vector that extends towards the lipophilic ribose pocket in the EGFR ATP binding site that is lined with multiple hydrophobic residues (Leu844, Val726, Cys797).[34] However, as shown in Table 6, expansion of the isopropyl group to a *sec*-butyl group within the current series did not improve potency (**20** and **21** vs **18**). Gratifyingly, superior metabolic stability for the more lipophilic **21** was observed in both in vitro human liver microsome and hepatocyte assays. Improved metabolic stability was only observed for the *S*-enantiomer when compared to the isopropyl analog, which suggests that the *N*-alkyl substitution may have affected the binding and/or activity of cytochrome P450 in a specific manner. The fact that **21** demonstrated appealing predicted human metabolic stability and excellent potency led us to compare the potential of this molecule to the reported clinical inhibitors.

Table 6. Optimization of *N*-alkyl group.

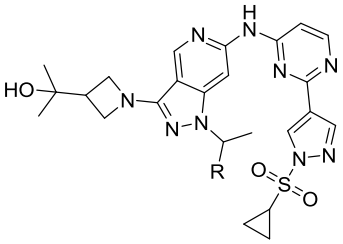

Cmpd	R	p-EGFR H1975 IC_{50} (μM)[a]	p-EGFR PC9-ER IC_{50} (μM)[a]	p-EGFR PC9 IC_{50} (μM)[a]	p-EGFR H292 IC_{50} (μM)[a]	HLM[b] / HHep[c] (ml min^{-1} kg^{-1})	MDCK A-B P_{app} (x 10^{-6} cm s^{-1})[d]	Kin Sol. (μM)[e]
18	CH_3	0.032	0.010	0.13	0.21	8.9/7.1	20	<1
20	CH_2CH_3 (*R*)	0.040	0.015	0.057	0.58	9.9/7.8	19	2
21	CH_2CH_3 (*S*)	0.027	0.0080	0.033	0.22	3.8/2.7	8.9	2

[a]Inhibition of EGFR phosphorylation. All IC_{50} data measurements reported are the geometric means of at least two independent experiments. H1975: Double mutant TMLR EGFR cell line. PC9-ER: Double mutant TMdel EGFR cell line. PC9: Activating mutant $del_{746\text{-}750}$ EGFR cell line. H292: Wild type EGFR cell line. [b]In vitro stability in human liver microsomes. [c]In vitro stability in cryopreserved human hepatocytes. [d]A-B, apical-to-basolateral. [e]Kinetic solubility at pH 7.4.

Compared to afatinib, an irreversible second generation EGFR inhibitor, **21** showed significantly reduced activity against wtEGFR (H292), which we believe to be important for safety considerations (Table 7). We were very pleased to see that, like osimertinib and in contrast to the first generation EGFR inhibitors (erlotinib and getifinib), **21** demonstrated excellent potency against both the activating and resistant EGFR mutants in the cellular mechanistic assays, yet without requiring a covalent interaction. In addition, **21** demonstrated strong anti-proliferative effect on the T790M mutant carrying H1975 cell line (IC_{50} = 0.361 μM) and the single activating mutant PC9 cell line (IC_{50} = 0.151 μM). Furthermore, compound **21** also showed good selectivity against other kinases when evaluated in a 225-kinase panel (12/225

kinases inhibited at >70% when tested at 0.1 μM, 61-fold over the TMLR Ki and 63-fold over the TMdel Ki; see supporting information).

Table 7. Comparison of cellular activity profiles.

	pEGFR IC_{50} (μM)[a]			
Cmpd	H1975	PC9-ER	PC9	H292
21	0.027	0.009	0.033	0.218
erlotinib	2.6	1.8	0.003	0.006
gefitinib	1.1	1.9	0.005	0.008
afatinib	0.010	0.035	0.001	0.004
osimertinib	0.043	0.017	0.031	0.483

[a]Inhibition of EGFR phosphorylation. All IC_{50} data measurements reported are the geometric means of at least two independent experiments. H1975: Double mutant TMLR cell line. PC9-ER: Double mutant TMdel cell line. PC9: Activating mutant $del_{746-750}$ cell line. H292: Wild type cell line.

With the encouraging in vitro pharmacological profile, we elected to further evaluate **21** in vivo. The pharmacokinetic profile of **21** is outlined in Table 8. In mouse, post intravenous and oral administration, the plasma clearance of **21** was determined to be 104 mL/min/kg with a bioavailability of 19%. In dogs, the plasma clearance was 13 mL/min/kg with an oral bioavailability of 30%. While high clearance at approximately liver blood flow was observed in mouse, the good correlation between in vivo clearance and in vitro clearance from liver microsomes in dog increased our confidence that **21** would have low clearance in human as the in vitro clearance measured from human liver microsomes and hepatocytes were both low.

Table 8. Pharmacokinetic parameters of **21**.

Species	**CL Liver microsomes**	**CL Hepatocytes (ml min^{-1} kg^{-1})[b]**	**iv Clp (ml min^{-1} kg^{-1}) / Vss (L kg^{-1})[c]**	**F%**

	(ml min^{-1} kg^{-1})[a]			
Mouse	66.5	52.6	104 / 3.4	19%[d]
Dog	12.6	6.5	13 / 6.9	30%[e]

[a]Clearance determined from liver microsomes. [b]Clearance determined from cryopreserved hepatocytes. [c] Clp = plasma clearance; Compound dosed iv (mouse = 5 mg kg^{-1}; dog = 1 mg kg^{-1}) as a solution in 10/35/55 ethanol/PEG/water solution. [d]Compound dosed po (25 mg kg^{-1}) as a solution in corn oil. [e]Compound dosed po (2 mg kg^{-1}) as a suspension in MCT.

Figure 5. Compound **21** was administered orally to H1975 tumor-bearing mice with either a 50 or 100 mg/kg single dose. Tumors were collected at indicated times and phosphorylation of EGFR, ERK, AKT was determined using commercially available MSD assays. Bars represent individual animals (four animals per group). Dotted line on the free plasma concentration plot shows the in vitro H1975 p-EGFR IC_{50}. Error bars represent the mean ± SD. Plasma concentrations of **21** were measured using liquid chromatography-tandem mass spectrometry assay, and free concentration was calculated using F_u of 0.009.

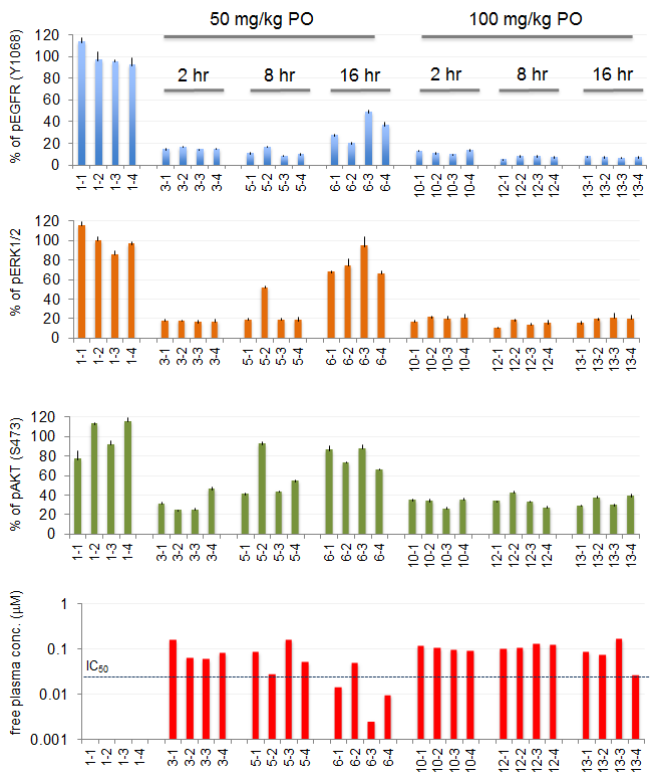

To examine its inhibitory effect on pEGFR levels in vivo, inhibitor **21** was studied in a mouse H1975 (TMLR) xenograft model (Figure 5). After single oral dose of **21** at 50 mg/kg, free plasma concentrations of **21** at or exceeding the in vitro p-EGFR IC_{50} of 0.027 μM were sustained over 8 h. When administered at 100 mg/kg, the coverage of p-EGFR IC_{50} was extended to the last measured time point of 16 h post dose. Corresponding knockdown of p-EGFR and the downstream effectors pERK1/2 and AKT levels were observed at those time points, suggesting target engagement in vivo.

Chemistry

Scheme 1.

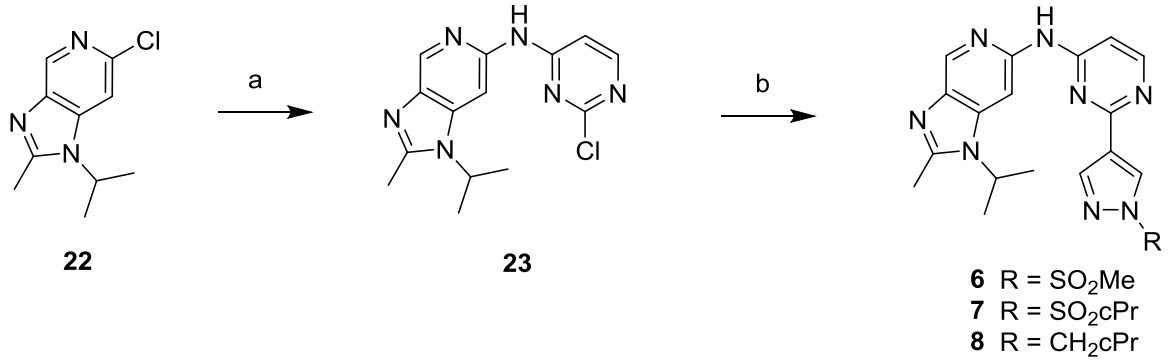

(a) 4-Amino-2-chloropyrimidine, $Pd_2(dba)_3$, XantPhos, Cs_2CO_3, 1,4-dioxane, 100 °C, 4 h, (26%); (b) **25**, **26** or **27**, Na_2CO_3, $Pd(Amphos)_2Cl_2$, CH_3CN, water, 100 °C, 3 h.

Scheme 2.

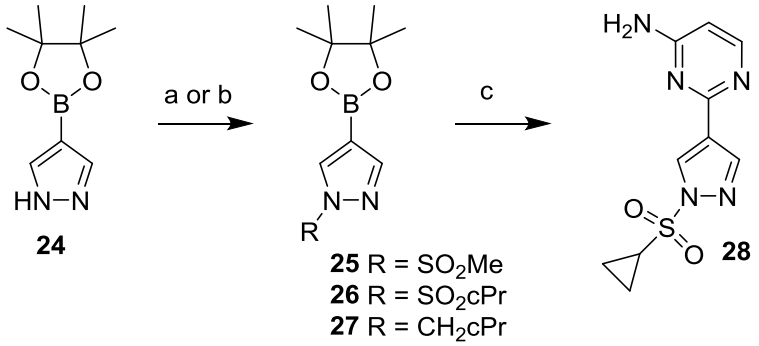

(a) For **25** and **26**, R-SO_2Cl, NaH, DMF, rt, 5 h; (b) For **27**, bromomethylcyclopropane, Cs_2CO_3, DMF, 60 °C, 12 h (45%); (c) For **26**, 2-chloropyrimidin-4-amine, Na_2CO_3, $Pd(Amphos)_2Cl_2$, CH_3CN, water, 100 °C, 2 h (85%).

Compounds **1**-**5** were prepared using procedures previously described.[34] Compounds **6**-**8** were synthesized as outlined in Scheme 1 and 2. Palladium-catalyzed coupling between chloro-azabenzimidazole **22**[34] and 2-chloropyrimidin-4-amine afforded intermediate **23**. Suzuki coupling between intermediate **23** and the corresponding 4-pyrazole pinacol boronic esters **25**-**27** yielded **6**-**8**. The 4-pyrazole pinacol boronic esters **25**-**27** were prepared via the alkylation or sulfonylation of the commercially available 4-(4,4,5,5-tetramethyl-1,3,2-dioxaborolan-2-yl)-1*H*-pyrazole (**24**).

Scheme 3.

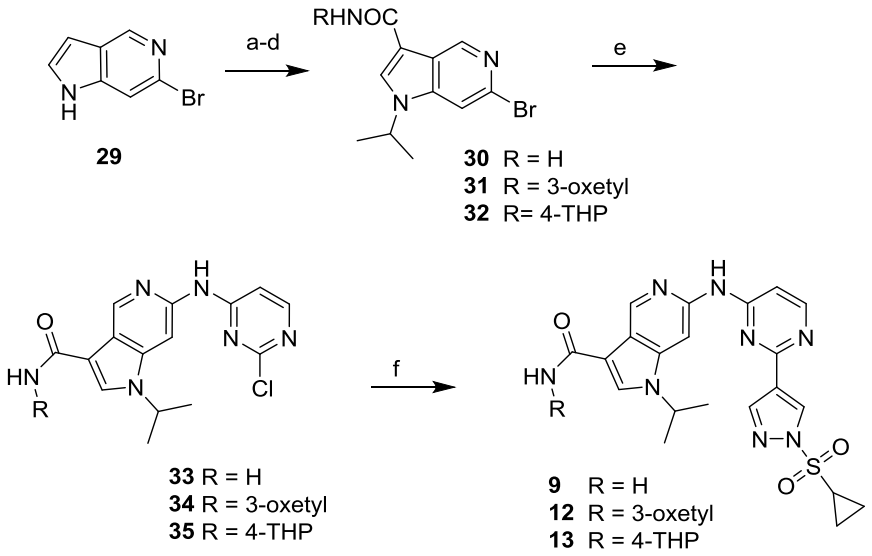

(a) 2-Bromopropane, NaH, DMF, 0 °C to rt, 2 h (quant.); (b) $POCl_3$, DMF, rt, 2 h (80%); (c) $NaOCl_2$, NaH_2PO_4, 2-methyl-2-butene, water, *t*-BuOH, rt, 18 h (94%); (d) NH_2R, HBTU, DIEA, DMF, rt, 40 min; (e) 4-amino-2-chloropyrimidine, Xantphos, $Pd_2(dba)_3$, Cs_2CO_3, dioxane, 120 °C, 6 h; (f) **26**, Na_2CO_3, $Pd(Amphos)_2Cl_2$, CH_3CN, water, 100 °C, 1 h.

Compounds **9**, **12** and **13** were prepared according to Scheme 3. A four-step sequence involving *N*-alkylation, Vilsmeier-Haack formylation, Pinnick oxidation, and amide bond formation efficiently advanced bromoazaindole **29** to intermediates **30-32**. Buchwald-Hartwig reactions between **30-32** and 2-chloropyrimidin-4-amine, followed by a Suzuki coupling with the pyrazole pinacol boronic ester **26**, afforded **9**, **12** and **13**.

Scheme 4.

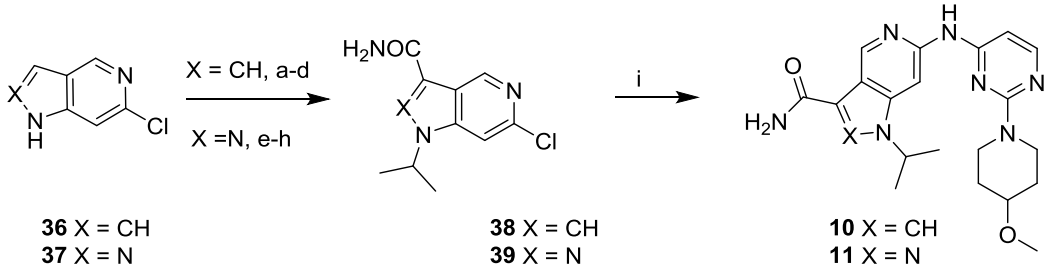

(a) 2-bromopropane, NaH, DMF, 0 °C to rt, 2 h (quant.); (b) $POCl_3$, DMF, rt, 2 h (80%); (c) $NaOCl_2$, NaH_2PO_4, 2-methyl-2-butene, water, *t*-BuOH, rt, 18 h (94%); (d) NH_2R, HBTU, DIEA, DMF, rt, 40 min; (e) I_2, K_2CO_3, DMF, rt, 1 h (quant.); (f) 2-bromopropane, NaH, DMF, 0 °C to rt, 2 h (81%); (g) $Pd(OAc)_2$, Et_3N, CH_3OH, CO, 65 °C, 3 h (40%); (h) i. $(CH_3)_3SnOH$, DCM, 60 °C, 4 h; ii. NH_4OH, HBTU, DIEA, DMF, rt, 20 min (25% over 2 steps); (i) 2-(4-methoxypiperidin-1-yl)pyrimidin-4-amine, chloro{[BrettPhos][2-(2-aminoethylphenyl]palladium(II)]}/[Brettphos] admixture, *t*-BuONa, t-BuOH, 120 °C, 3 h.

Compounds **10** and **11** were synthesized according to Scheme 4. Azaindole **38** was prepared via the four step sequence described above starting from 6-chloro-5-azaindole (**36**). Iodination and alkylation of 6-chloro-5-azaindazole[34] (**37**), followed by methoxycarbonylation and amide bond synthesis, afforded azaindazole **39**. Palladium-catalyzed coupling of **38** or **39** with 2-(4-methoxypiperidin-1-yl)pyrimidin-4-amine yielded **10** and **11**.

Scheme 5.

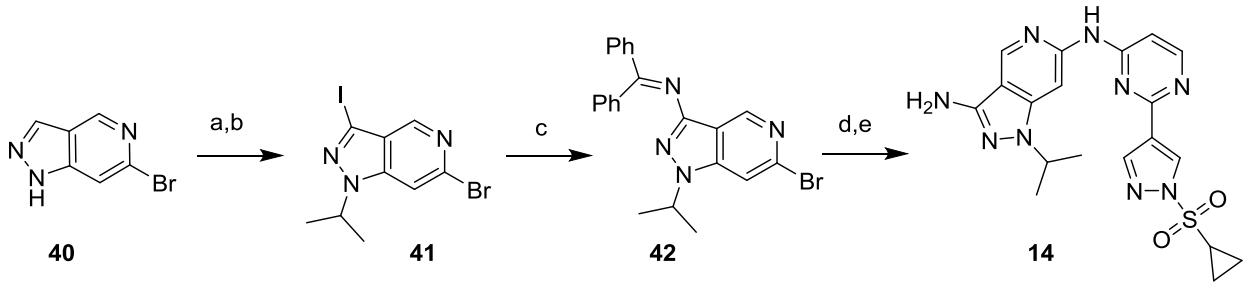

(a) I_2, K_2CO_3, DMF, rt (quant.); (b) 2-bromopropane, NaH, DMF, 0 °C to RT (44%); (c) Benzophenone imine, Cs_2CO_3, $Pd_2(dba)_3$, Xantphos, 1,4-dioxane, 90 °C (58%); (d) **28**, $Pd_2(dba)_3$, Xantphos, Cs_2CO_3, 1,4-dioxane, 100 °C (50%); (e) $NH_2OH{\cdot}HCl$, NaOAc, rt (14%).

Scheme 6.

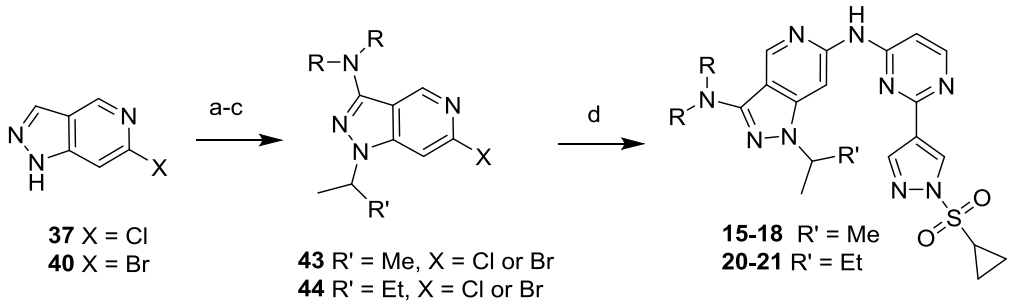

(a) I_2, K_2CO_3, DMF, rt; (b) 2-bromopropane or 2-bromobutane, NaH, DMF, 0 °C to rt (quant.); (c) HNR_2, CuI, L-proline, K_2CO_3, 90 °C, 3.5 h; (d) **28**, $Pd_2(dba)_3$, XPhos, Cs_2CO_3, 1,4-dioxane, 100 °C.

Compound **14** was prepared according to Scheme 5. Iodination and *N*-alkylation of 6-bromo-5-azaindazole (**40**) afforded **41**. Installation of the protected 3-amino group was accomplished by a palladium-catalyzed coupling using benzophenone imine. Subsequent coupling with **28**, followed by imine cleavage gave inhibitor **14**. Similarly, inhibitors **15-18** and **20-21** were synthesized according to Scheme 6. Iodination and *N*-alkylation of the commercially available **37** or **40** followed by copper-mediated amination yielded intermediates **43-44**. Subsequent palladium-catalyzed amination using the previously described aminopyrimidines **28** afforded the inhibitors **15-18** and **20-21**. Chiral separation of **20** and **21** was achieved by using chiral supercritical fluid chromatography. Absolute stereochemistry of **21** was assigned by crystallography (see supporting information).

Scheme 7.

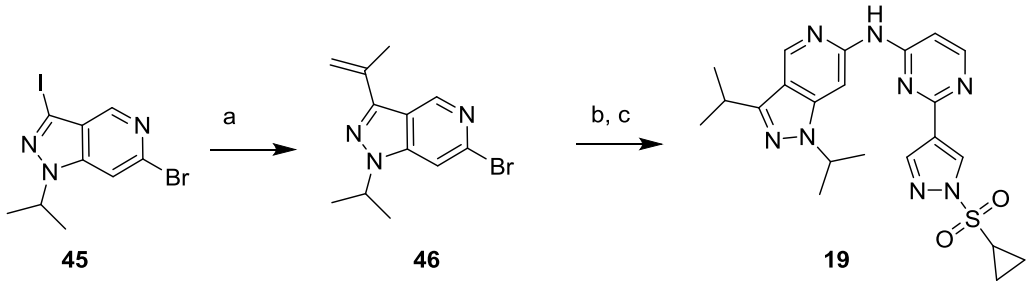

(a) 4,4,5,5-tetramethyl-2-(prop-1-en-2-yl)-1,3,2-dioxaborolane, $Pd(dppf)Cl_2$, Na_2CO_3, KOAc, water, CH_3CN, 100 °C, μW (45%); (b) **28**, $Pd_2(dba)_3$, XPhos, Cs_2CO_3, 1,4-dioxane, 100 °C (65%); (c) H_2, $Pd(OH)_2/C$, rt (56%).

The synthesis of **19** began with a Suzuki coupling to yield isopropene **46** (Scheme 7). Buchwald-Hartwig coupling between **46** and **28**, followed by hydrogenation afforded **19**.

Conclusions

By using a structure-based design approach, we identified a novel, non-covalent EGFR inhibitor that exhibits excellent activity against both the activating and resistance mutants of the receptor. In sparing the wild type form of EGFR, a wider therapeutic window can be anticipated relative to first and second generation inhibitors. Without the reliance on a covalent interaction with Cys797, inhibitors of this type should be able to achieve the efficacy of the covalent inhibitors without being subject to the emerging C797S resistance mutation. With strong pathway knock-down in vivo and low predicted human clearance, compound **21** shows excellent potential for the treatment of EGFR-mutant NSCLC. Further in vivo evaluation of compound **21** will be disclosed in due course.

EXPERIMENTAL SECTION

Synthesis. General methods: ^1H NMR spectra were recorded at ambient temperature using either a Varian Unity Inova (400MHz) spectrometer with a triple resonance 5mm probe, an Avance III (300 MHz) spectrometer or a Bruker Ultrashield (400 MHz or 500 MHz) spectrometer. Chemical shifts are expressed in ppm relative to tetramethylsilane. The following abbreviations have been used: br = broad signal, s = singlet, d = doublet, dd = double doublet, t = triplet, q = quartet, m =

multiplet. Microwave experiments were carried out using a CEM Discover, Smith Synthesiser or a Biotage Initiator 60™, which uses a single-mode resonator and dynamic field tuning, both of which give reproducibility and control. Temperatures from 40-250 °C can be achieved and pressures of up to 30 bar can be reached. HPLC/UPLC - Mass Spectrometry experiments to determine retention times and associated mass ions were performed using various methods which are fully described in the Supporting Information. All final compounds were assessed for purity by UPLC and found to be ≥95% purity. Diastereomeric and enantiomeric purity of final compounds was assessed by UPLC and SFC respectively and found to be >95% de and >95% ee. Experimental procedures for selected inhibitors are described below. Experimental procedures for all inhibitors are provided in the supporting information. Compounds **1-5** were prepared as previously described.[34, 35]

***N*-(2-(1-(cyclopropylsulfonyl)-1*H*-pyrazol-4-yl)pyrimidin-4-yl)-1-isopropyl-2-methyl-1*H*-imidazo[4,5-*c*]pyridin-6-amine(7)**

*1-(Cyclopropylsulfonyl)-4-(4,4,5,5-tetramethyl-1,3,2-dioxaborolan-2-yl)-1H-pyrazole (**26**).* To a solution of 4-pyrazoleboronic acid pinacol ester (1.02 g, 5.26 mmol) in DMF (15 mL) was added sodium hydride (60%, 0.32 g, 8 mmol) and cyclopropylsulfonyl chloride (0.8 g, 5.78 mmol). The reaction was stirred at room temperature for 5 h. The mixture was then diluted with brine and extracted with EtOAc (3x). The combined extracts were washed with brine, dried over sodium sulfate, filtered and concentrated. The crude material was purified by flash chromatography (0-100% EtOAc in heptanes) to give the title compound (0.8 g, 50%). ^{1}H NMR (400 MHz, $CDCl_3$) δ 8.29 (s, 1H), 8.01 (s, 1H), 2.77 (m, 1H), 1.48 (m, 2H), 1.33 (s, 12H), 1.16 (m, 2H).

*N-(2-chloropyrimidin-4-yl)-1-isopropyl-2-methyl-1H-imidazo[4,5-c]pyridin-6-amine (**23**).* Into a 250 mL 3-necked round-bottom flask purged and maintained with nitrogen, was added a solution of 6-bromo-1-isopropyl-2-methyl-1*H*-imidazo[4,5-*c*]pyridine[34] (3.50 g, 13.0 mmol) in 1,4-dioxane (70.0 mL), 2-chloropyrimidin-4-amine (1.70 g, 13.1 mmol), XantPhos (1.70 g, 2.94 mmol), $Pd_2(dba)_3{\cdot}CHCl_3$ (1.70 g, 1.64 mmol) and Cs_2CO_3 (11.0 g, 33.7 mmol). The resulting mixture was stirred at 100 °C for 4 h. The mixture was cooled to room temperature, the solids were removed by filtration and the filtrate was concentrated under vacuum. The residue was purified by silica gel flash chromatography (DCM/MeOH, 50:1) to afford the title compound (1.10 g, 26.1%) as a yellow solid. LCMS (ESI): $[M+H]^+$ = 303. ^{1}HNMR (300Hz, DMSO-d_6): δ 10.55 (s, 1H), 8.57 (s, 1H), 8.26 (d, *J* = 5.7 Hz, 1H), 8.13 (s, 1H), 7.48 (s, 1H), 4.72-4.68 (m, 1H), 2.58 (s, 3H), 1.57 (d, *J* = 6.9, 6H).

*N-(2-(1-(cyclopropylsulfonyl)-1H-pyrazol-4-yl)pyrimidin-4-yl)-1-isopropyl-2-methyl-1H-imidazo[4,5-c]pyridin-6-amine (**7**).* To a reaction vial was added *N*-cyclopropylsulfonyl-4-pyrazoleboronic acid pinacol ester (0.56 g, 1.8 mmol), *N*-(2-chloropyrimidin-4-yl)-1-isopropyl-2-methyl-1*H*-imidazo[4,5-c]pyridin-6-amine (0.56 mg, 1.8 mmol), $Pd(Amphos)_2Cl_2$ (65 mg, 0.092 mmol), a 2 M aqueous solution of Na_2CO_3 (1.4 mL, 2.8 mmol) and acetonitrile (2.5 mL). The mixture was degassed by nitrogen bubbling for 20 min. The reaction vial was sealed and stirred at 100 °C in an oil bath for 3 h. The reaction mixture was cooled to room temperature, filtered and concentrated. The crude product was purified by reverse phase HPLC to give the title compound (41 mg, 5 %). LCMS (ESI): $[M+H]^+$ 439.2. ^{1}H NMR (400 MHz, DMSO-d_6) δ 10.16 (s, 1H), 8.66 (s, 1H), 8.56 (d, *J* = 0.8 Hz, 1H), 8.47 (d, *J* = 0.5 Hz, 1H), 8.39 (m, 2H), 7.24 (s, 1H), 4.78 (m, 1H), 2.58 (s, 3H), 1.63 (d, *J* = 6.9 Hz, 6H), 1.38 – 1.21 (m, 4H).

6-((2-(1-(Cyclopropylsulfonyl)-1*H*-pyrazol-4-yl)pyrimidin-4-yl)amino)-1-isopropyl-1*H*-pyrrolo[3,2-*c*]pyridine-3-carboxamide (9).

6-Bromo-1-isopropyl-1H-pyrrolo[3,2-c]pyridine. To a solution of 6-bromo-5-azaindole (1.0 g, 4.9 mmol) in DMF (8 mL) was added 60% sodium hydride (0.23 g, 5.8 mmol) at 0 ºC. The mixture was stirred 0 ◦C for 5 min prior to the addition of 2-bromopropane (0.7 mL, 7 mmol). The reaction was stirred at room temperature for 2 h. The reaction was then quenched by pouring onto a saturated aqueous solution of NH_4Cl. The product was extracted with EtOAc (3x). The combined extracts were washed with brine, dried over sodium sulfate, filtered and concentrated. The crude product was purified by silica gel flash chromatography (0-100 % EtOAc in heptane) to give the title compound (1.5 g, quant.). LCMS (ESI): $[M+H]^+ = 239.2$.

6-Bromo-1-isopropyl-1H-pyrrolo[3,2-c]pyridine-3-carbaldehyde. To cooled (0 ◦C) DMF (40 mL) was added $POCl_3$ (3.0 mL, 31 mmol). The reaction was stirred at 0 ºC for 20 min. A solution of 6-bromo-1-isopropyl-1*H*-pyrrolo[3,2-*c*]pyridine (4.9 mmol) in DMF (1 mL) was added drop wise at room temperature. The reaction was stirred at 70 ◦C for 2 h. The mixture was then slowly neutralized by pouring onto a saturated aqueous $NaHCO_3$ solution. The product was extracted with EtOAc (3x). The combined organic extracts were washed with saturated aqueous $NaHCO_3$ and brine, dried over sodium sulfate, filtered and concentrated. The crude product was purified by silica gel flash chromatography (0-100 % EtOAc in heptane) to give the title compound (1.34 g, 80%). LCMS (ESI): $[M+H]^+ = 267.3$.

*6-Bromo-1-isopropyl-1H-pyrrolo[3,2-c]pyridine-3-carboxamide (**30**).* To a solution of 6-bromo-1-isopropyl-1*H*-pyrrolo[3,2-*c*]pyridine-3-carbaldehyde (1.3 g, 4.9 mmol) in *t*-BuOH (10 mL) was added 2-methyl-2-butene (2 M in THF, 4.1 mL, 49 mmol). A solution of sodium chlorite (1.1 g, 9.7 mmol) and monosodium phosphate (5.8 g, 49 mmol) in water (15 mL) was

then added. The reaction was stirred at room temperature for 18 h. The mixture was then diluted with brine and extracted with EtOAc (3x). The combined extracts were washed with brine, dried over sodium sulfate, filtered and concentrated to give the title compound (1.3 g, 94%). The crude material was used without further purification.

To a solution of the crude 6-bromo-1-isopropyl-1*H*-pyrrolo[3,2-*c*]pyridine-3-carboxylic acid (1.25 g, 4.4 mmol) in DMF (10 mL) was added DIPEA (1.2 mL, 6.6 mmol) and HBTU (2.64 g, 6.62 mmol). The mixture was stirred at room temperature for 15 min before the addition of ammonium hydroxide (10 mL). The resulting mixture was stirred vigorously for 1 h. The mixture was then diluted with brine and extracted with EtOAc (3x). The combined extracts were washed with brine, dried over sodium sulfate, filtered and concentrated. The crude material was purified by silica gel flash chromatography (0-10 % MeOH in DCM) to give the title compound (0.72 g, 58%). LCMS (ESI): $[M+H]^+ = 282.3$.

*6-((2-Chloropyrimidin-4-yl)amino)-1-isopropyl-1H-pyrrolo[3,2-c]pyridine-3-carboxamide (**33**).* To a pressure reaction vessel was added 6-bromo-1-isopropyl-1*H*-pyrrolo[3,2-*c*]pyridine-3-carboxamide (0.15 g, 0.53 mmol), 4-amino-2-chloropyrimidine (70 mg, 0.53 mmol), Xantphos (32 mg, 0.053 mmol), $Pd_2(dba)_3$ (25 mg, 0.027 mmol), Cs_2CO_3 (0.35 g, 1.1 mmol) and 1,4-dioxane (2 mL). The mixture was degassed by nitrogen bubbling for 20 min. The reaction vessel was then sealed and stirred at 120 °C for 6 h. The reaction was then filtered and concentrated. The crude product was purified by silica gel flash chromatography (0-10 % MeOH in DCM) to give the title compound (0.70 g, 40%). LCMS (ESI): $[M+H]^+ = 331$.

*6-((2-(1-(Cyclopropylsulfonyl)-1H-pyrazol-4-yl)pyrimidin-4-yl)amino)-1-isopropyl-1H-pyrrolo[3,2-c]pyridine-3-carboxamide (**9**).* To a glass vial was added 1-(cyclopropylsulfonyl)-4-(4,4,5,5-tetramethyl-1,3,2-dioxaborolan-2-yl)-1*H*-pyrazole (95 mg, 0.30 mmol), 6-((2-

chloropyrimidin-4-yl)amino)-1-isopropyl-1*H*-pyrrolo[3,2-*c*]pyridine-3-carboxamide (50 mg, 0.15 mmol), $Pd(Amphos)_2Cl_2$ (5 mg, 0.008 mmol), a 2 M aqueous solution of Na_2CO_3 (0.11 mL, 0.23 mmol) and acetonitrile (2.5 mL). The mixture was degassed by nitrogen bubbling for 20 min. The reaction vial was sealed and stirred at 100 °C in an oil bath for 1 h. The reaction mixture was cooled to room temperature, filtered and concentrated. The crude product was purified by reverse phase HPLC and lyophilized to give the title compound (20 mg, 30%). LCMS (ESI): $[M+H]^+$ = 467.2. ^{1}H NMR (400 MHz, DMSO-d_6) δ 10.27 (s, 1H), 9.08 (t, *J* = 2.4 Hz, 1H), 8.70 (d, *J* = 0.5 Hz, 1H), 8.50 (s, 1H), 8.47 (d, *J* = 0.5 Hz, 1H), 8.37 (d, *J* = 5.9 Hz, 1H), 8.23 (s, 1H), 7.49 (s, 1H), 7.11 (s, 1H), 6.97 (d, *J* = 8.7 Hz, 1H), 6.63 (d, *J* = 8.8 Hz, 1H), 4.80 (m, 1H), 1.56 (d, *J* = 6.7 Hz, 6H), 1.40 – 1.31 (m, 2H), 1.30 – 1.23 (m, 2H).

***N*-(2-(1-(cyclopropylsulfonyl)-1*H*-pyrazol-4-yl)pyrimidin-4-yl)-1-isopropyl-3-morpholino-1*H*-pyrazolo[4,3-*c*]pyridin-6-amine (15).**

4-(6-bromo-1-isopropyl-1H-pyrazolo[4,3-c]pyridin-3-yl)morpholine. A mixture of 6-bromo-3-iodo-1-isopropyl-1*H*-pyrazolo[4,3-*c*]pyridine (1 g, 2.73 mmol), CuI (103.8 mg, 0.550 mmol), L-proline (94.3 mg, 0.820 mmol), K_2CO_3 (943 mg, 6.82 mmol) and morpholine (713 mg, 8.19 mmol) in DMF (10 mL) was irradiated with microwave radiation for 2 h at 100 °C under an atmosphere of nitrogen. The resulting solution was diluted with water and extracted with ethyl acetate. The organic extract was washed with brine then dried over anhydrous sodium sulfate and concentrated *in vacuo*. The crude product was purified by silica gel flash chromatography (10% EtOAc in petroleum ether) to afford the title compound (140 mg, 16%) as a white solid. LCMS (ESI): [M+H]+ = 325/327.

*2-(1-(Cyclopropylsulfonyl)-1H-pyrazol-4-yl)pyrimidin-4-amine (**28**).* To a reaction vessel was added $Pd(Amphos)_2Cl_2$ (370 mg, 0.50 mmol), 1-(cyclopropylsulfonyl)-4-(4,4,5,5-tetramethyl-

1,3,2-dioxaborolan-2-yl)-1*H*-pyrazole (1.5 g, 4.3 mmol), 2-bromopyrimidin-4-amine (880 mg, 5.0 mmol), a 2 M aqueous solution of Na_2CO_3 in water (5.0 mL, 10 mmol) and acetonitrile (8.4 mL, 160 mmol). The reaction vessel was sealed and heated to 100 °C in an oil bath. After 2 h, the reaction was cooled to room temperature, diluted with saturated aqueous $NaHCO_3$, and extracted with EtOAc (3x). The combined organic extracts were washed with brine, dried over anhydrous sodium sulfate, filtered and concentrated *in vacuo*. The crude product was then purified via silica gel flash chromatography (0%-10% MeOH in DCM) to give the title compound (1129 g, 85%) as a yellow solid. LCMS (ESI) $[M+H]^+ = 266.1$; ^{1}H NMR (400 MHz, DMSO-d_6) δ 8.86 (s, 1H), 8.44 (s, 1H), 8.27 (d, *J* = 5.1 Hz, 1H), 7.06 (d, *J* = 5.1 Hz, 1H), 6.63 (s, 2H), 3.22 (m, 1H), 1.38 – 1.29 (m, 2H), 1.28 – 1.19 (m, 2H).

*N-(2-(1-(cyclopropylsulfonyl)-1H-pyrazol-4-yl)pyrimidin-4-yl)-1-isopropyl-3-morpholino-1H-pyrazolo[4,3-c]pyridin-6-amine (**15**).* To a reaction vessel was added 4-[6-bromo-1-(propan-2-yl)-1*H*-pyrazolo[4,3-*c*]pyridin-3-yl]morpholine (100 mg, 0.310 mmol), Xantphos (35 mg, 0.060 mmol), $Pd_2(dba)_3$ (28.0 mg, 0.030 mmol), Cs_2CO_3 (251 mg, 0.770 mmol), 2-[1-(cyclopropanesulfonyl)-1*H*-pyrazol-4-yl]pyrimidin-4-amine (97.8 mg, 0.370 mmol) and 1,4-dioxane (5 mL). The mixture was degassed by nitrogen bubbling for 5 min. The resulting solution was stirred for 3 h at 90 °C then cooled to room temperature. The reaction mixture was concentrated *in vacuo*. The crude product was purified via silica gel flash chromatography (0%-4% MeOH in DCM) to give the title compound (25.6 mg, 16%) as an off-white solid. LCMS (ESI): $[M+H]^+$ 510.1. ^{1}H NMR (300 MHz, DMSO-d_6): δ 10.37 (s, 1H), 8.91 (s, 1H), 8.70 (s, 1H), 8.47 (s, 1H), 8.42-8.40 (d, *J* = 6.0 Hz, 1H), 8.34 (s, 1H), 7.12-7.10 (d, *J* = 6.0 Hz, 1H), 4.77-4.72 (m, 1H), 3.81-3.78 (m, 4H), 3.42-3.39 (m, 4H), 3.31-3.26 (m, 1H), 1.48-1.46 (d, *J* = 6.6 Hz, 6H), 1.35-1.32 (m, 2H), 1.29-1.23 (m, 2H).

2-(1-(6-((2-(1-(Cyclopropylsulfonyl)-1*H*-pyrazol-4-yl)pyrimidin-4-yl)amino)-1-isopropyl-1*H*-pyrazolo[4,3-*c*]pyridin-3-yl)azetidin-3-yl)propan-2-ol (18).

6-Chloro-3-iodo-1H-pyrazolo[4,3-c]pyridine. To a solution of 6-chloro-1*H*-pyrazolo[4,3-*c*]pyridine (5.2 g, 34 mmol) in DMF (75 mL) was added K_2CO_3 (5.7 g, 41 mmol) and iodine (4.3 g, 41 mmol). The reaction was stirred at room temperature. After 4 h, additional iodine (4.3 g, 17 mmol) and K_2CO_3 (2.3 g, 17 mmol) were added. After 16 h of stirring at room temperature, the reaction was diluted with saturated aqueous $NaHCO_3$ and extracted with EtOAc (3x). The combined organic extracts were washed with brine, dried over anhydrous sodium sulfate, filtered, concentrated *in vacuo* and purified via silica gel flash chromatography (0%-100% EtOAc in heptane) to give the title compound (7.5 g, 79%). LCMS (ESI) $[M+H]^+$ = 280. ^{1}H NMR (400 MHz, DMSO-d_6) δ 14.02 (br, 1H), 8.63 (br, 1H), 7.69 (s, 1H).

6-Chloro-3-iodo-1-isopropyl-1H-pyrazolo[4,3-c]pyridine. To a solution of 6-chloro-3-iodo-1*H*-pyrazolo[4,3-*c*]pyridine (1.5 g, 5.4 mmol) in DMF (8 mL) was added sodium hydride (60 wt% dispersion in mineral oil, 260 mg, 6.4 mmol) at 0 °C. The reaction was stirred at 0 °C for 5 min before adding 2-bromopropane (0.76 mg, 8.1 mmol). The reaction was warmed to room temperature and stirred for 2 h, after which the reaction was diluted with saturated aqueous NH_4Cl, and extracted with EtOAc (3x). The combined organic extracts were washed with brine, dried over anhydrous sodium sulfate, filtered, and concentrated. The crude product was purified via silica gel flash chromatography (0%-100% EtOAc in heptanes) to provide the title compound (1390 mg, 81%) as a pale yellow solid. LCMS (ESI) $[M+H]^+$ = 322.1; ^{1}H NMR (400 MHz, $CDCl_3$) δ 8.56 (s, 1H), 7.34 (s, 1H), 4.78-4.71 (m, 1H), 1.60 (d, J = 6.8 Hz, 6H).

2-(1-(6-Chloro-1-isopropyl-1H-pyrazolo[4,3-c]pyridin-3-yl)azetidin-3-yl)propan-2-ol. To a reaction vessel was added 6-chloro-3-iodo-1-(propan-2-yl)-1*H*-pyrazolo[4,3-*c*]pyridine (300 mg,

0.930 mmol), $Pd_2(dba)_3$ (85.4 mg, 0.090 mmol), XantPhos (108 mg, 0.190 mmol), Cs_2CO_3 (608 mg, 1.87 mmol), 2-(azetidin-3-yl)propan-2-ol (107 mg, 0.930 mmol) and 1,4-dioxane (8 mL). The mixture was stirred for 6 h at 100 °C. The reaction mixture was cooled to room temperature and the solids were removed by filtration. The filtrate was concentrated *in vacuo*. The crude product was purified via silica gel flash chromatography (0%-50% EtOAc in petroleum ether) to provide the title compound (130 mg, 45%) as a white solid. LCMS (ESI): $[M+H]^+$ = 309.

*2-(1-(6-((2-(1-(Cyclopropylsulfonyl)-1H-pyrazol-4-yl)pyrimidin-4-yl)amino)-1-isopropyl-1H-pyrazolo[4,3-c]pyridin-3-yl)azetidin-3-yl)propan-2-ol (**18**).* In a reaction vessel was placed 2-[1-[6-chloro-1-(propan-2-yl)-1*H*-pyrazolo[4,3-*c*]pyridin-3-yl]azetidin-3-yl]propan-2-ol (120 mg, 0.390 mmol), $Pd_2(dba)_3$ (35.6 mg, 0.04 mmol), Xantphos (45.0 mg, 0.08 mmol), Cs_2CO_3 (253 mg, 0.780 mmol), 2-[1-(cyclopropanesulfonyl)-1*H*-pyrazol-4-yl]pyrimidin-4-amine (103 mg, 0.390 mmol) and 1,4-dioxane (8 mL). The mixture was heated with microwave radiation for 45 min at 160 °C. The reaction was filtered and concentrated *in vacuo*. The crude product was purified via silica gel flash chromatography (0%-10% methanol in DCM) to provide the title compound (26.8 mg, 13%) as a light yellow solid. LCMS (ESI): $[M+H]^+$ = 538.1. ^{1}H NMR (300 MHz, DMSO-d_6): δ 10.32 (s, 1H), 8.69 (s, 1H), 8.61 (s, 1H), 8.47 (s , 1H), 8.40 (d, *J* = 5.6 Hz,1H), 8.27 (s, 1H), 7.13 (d, *J* = 5.6 Hz, 1H), 4.71-4.67 (m, 1H), 4.44 (s, 1H), 4.07-4.01 (m, 4H), 3.29-3.27 (m, 1H), 2.84-2.81 (m, 1H), 1.46 (d, *J* = 6.8 Hz, 6H), 1.34 (m, 2H), 1.30-1.23 (m, 2H), 1.08 (s , 6H).

(*R*)-2-(1-(1-(*sec*-Butyl)-6-((2-(1-(cyclopropylsulfonyl)-1*H*-pyrazol-4-yl)pyrimidin-4-yl)amino)-1*H*-pyrazolo[4,3-*c*]pyridin-3-yl)azetidin-3-yl)propan-2-ol (20) and (*S*)-2-(1-(1-(*sec*-Butyl)-6-((2-(1-(cyclopropylsulfonyl)-1*H*-pyrazol-4-yl)pyrimidin-4-yl)amino)-1*H*-pyrazolo[4,3-*c*]pyridin-3-yl)azetidin-3-yl)propan-2-ol (21)

(±)-1-(sec-Butyl)-6-chloro-3-iodo-1H-pyrazolo[4,3-c]pyridine. To a solution of 6-chloro-3-iodo-1*H*-pyrazolo[4,3-*c*]pyridine (3.5 g, 13 mmol) in DMF (25 mL) was added sodium hydride (60 wt% dispersion in mineral oil, 0.6 g, 15 mmol). The reaction mixture was stirred at room temperature for 10 min prior to the addition of 2-bromobutane (2.7 mL, 25 mmol). The reaction was stirred at room temperature for 5 h, diluted with brine and extracted with EtOAc (3x). The combined organic extracts were washed with brine, dried over anhydrous sodium sulfate, filtered and concentrated *in vacuo*. The crude product was purified via silica gel flash chromatography (0%-100% EtOAc in heptane) to give the title compound (3.6 g, 86%). LCMS (ESI): $[M+H]^+$ = 336. ^{1}H NMR (400 MHz, $CDCl_3$) δ 8.56 (s, 1H), 7.31 (s, 1H), 4.54 – 4.35 (m, 1H), 2.15 – 1.99 (m, 1H), 1.98 – 1.81 (m, 1H), 1.61 – 1.49 (m, 3H), 0.79 (t, *J* = 7.4 Hz, 3H).

(±)-2-[1-(6-Chloro-1-sec-butyl-pyrazolo[4,3-c]pyridin-3-yl)azetidin-3-yl]propan-2-ol. To a reaction vessel was added 6-chloro-3-iodo-1-isopropyl-1*H*-pyrazolo[4,3-*c*]pyridine (1.0 g, 1.4 mmol), 2-(azetidin-3-yl)propan-2-ol (0.41g, 3.6 mmol), K_2CO_3 (1.4 g, 10 mmol), L-proline (0.17 g, 1.5 mmol), copper(I) iodide (0.28 g, 1.5 mmol) and DMF (8 mL). The reaction was degassed by nitrogen bubbling for 20 min. The reaction vessel was sealed and stirred at 90 °C. After 3.5 h, the reaction was cooled to room temperature, filtered and extracted with EtOAc (3x). The combined organic extracts were washed with brine, dried over anhydrous sodium sulfate, filtered and concentrated *in vacuo*. The crude product was purified via silica gel flash chromatography (0%-100% EtOAc in heptane) to give the title compound (0.45 g, 47%). LCMS (ESI): $[M+H]^+$ = 323.3.

*(R)-2-(1-(1-(sec-Butyl)-6-((2-(1-(cyclopropylsulfonyl)-1H-pyrazol-4-yl)pyrimidin-4-yl)amino)-1H-pyrazolo[4,3-c]pyridin-3-yl)azetidin-3-yl)propan-2-ol (**20**) and (S)-2-(1-(1-(sec-Butyl)-6-((2-(1-(cyclopropylsulfonyl)-1H-pyrazol-4-yl)pyrimidin-4-yl)amino)-1H-pyrazolo[4,3-c]pyridin-*

*3-yl)azetidin-3-yl)propan-2-ol (**21**)*. To a reaction vessel was added (±)-2-[1-(6-chloro-1-*sec*-butyl-pyrazolo[4,3-*c*]pyridin-3-yl)azetidin-3-yl]propan-2-ol (0.25 g, 0.68 mmol), 2-(1-(cyclopropylsulfonyl)-1*H*-pyrazol-4-yl)pyrimidin-4-amine (0.18 g, 0.68 mmol), Cs_2CO_3 (0.44 g, 1.4 mmol), 2-dicyclohexylphosphino-2′,4′,6′-triisopropylbiphenyl (66 mg, 0.14 mmol), tris(dibenzylideneacetone)dipalladium(0) (31 mg, 0.034 mmol) and 1,4-dioxane (3 mL). The reaction was degassed by nitrogen bubbling for 20 min and heated at 100 °C for 3 h. The reaction mixture was cooled to room temperature, filtered and concentrated *in vacuo*. The products were purified and the enantiomers were separated by chiral supercritical fluid chromatography to give the title compounds (absolute stereochemistry assigned by x-ray structure of **21** complexed with EGFR TMLR; see Supporting Information): *(R)-2-(1-(1-(sec-Butyl)-6-((2-(1-(cyclopropylsulfonyl)-1H-pyrazol-4-yl)pyrimidin-4-yl)amino)-1H-pyrazolo[4,3-c]pyridin-3-yl)azetidin-3-yl)propan-2-ol* (**20**, 43.4 mg, 12%): LCMS $[M+H]^+$ = 552.3. ^{1}H NMR (400 MHz, DMSO-d_6) δ 10.33 (s, 1H), 8.69 (s, 1H), 8.62 (d, *J* = 1.0 Hz, 1H), 8.48 (s, 1H), 8.40 (d, *J* = 5.9 Hz, 1H), 8.26 (s, 1H), 7.14 (d, *J* = 5.9 Hz, 1H), 4.46 (s, 1H), 4.35-4.44 (m, 1H), 4.01-4.08 (m, 4H), 3.26-3.32 (m, 1H), 2.79-2.86 (m, 1H), 1.87 – 1.99 (m, 1H), 1.73 – 1.85 (m, 1H), 1.45 (d, *J* = 6.6 Hz, 3H), 1.23-1.36 (m, 4H), 1.09 (s, 6H), 0.73 (t, *J* = 7.3 Hz, 3H). *(S)-2-(1-(1-(sec-Butyl)-6-((2-(1-(cyclopropylsulfonyl)-1H-pyrazol-4-yl)pyrimidin-4-yl)amino)-1H-pyrazolo[4,3-c]pyridin-3-yl)azetidin-3-yl)propan-2-ol* (**21**, 40.1 mg, 11%): $[M+H]^+$ = 552.3. ^{1}H NMR (400 MHz, DMSO-d_6) δ 10.33 (s, 1H), 8.69 (s, 1H), 8.62 (d, *J* = 1.0 Hz, 1H), 8.47 (s, 1H), 8.41 (d, *J* = 5.9 Hz, 1H), 8.26 (s, 1H), 7.12 (d, *J* = 5.9 Hz, 1H), 4.46 (s, 1H), 4.37-4.42 (m, 1H), 4.01-4.8 (m, 4H), 3.26-3.32 (m, 1H), 2.79-2.87 (m ,1H), 1.88-1.99 (m, 1H), 1.76-1.83 (m, 1H), 1.45 (d, *J* = 6.6 Hz, 3H), 1.24-1.37 (m, 4H), 1.08 (s, 6H), 0.72 (t, *J* = 7.3 Hz, 3H). ^{13}C NMR (100 MHz,

DMSO-d_6) δ 159.96, 158.34, 156.23, 153.02, 149.46, 145.18, 144.28, 143.45, 131.73, 126.07, 109.53, 107.20, 90.88, 68.30, 55.55, 54.06, 42.24, 31.24, 29.14, 27.11, 20.39, 11.53, 7.29.

Enzymatic Assays. Enzymatic assays were carried out as previously described.[34,35] All enzymatic data reported are the geometric means of at least two independent experiments.

Cellular Assays. All pEGFR MSD and H1975 proliferation assays were carried out as previously described.[34,35]

In vitro microsome and hepatocyte metabolic stability assays. Experiments were carried out as previously described.[39] Values shown are for predicted hepatic clearance using intrinsic clearance and a conversion factor for liver blood flow to predict hepatic clearance.[40] Cl_{hep}= $(Q.Cl_{int})/(Q+Cl_{int})$ where Cl_{hep}= predicted hepatic clearance, Q= liver blood flow and Cl_{int}= intrinsic clearance. Liver blood flow values in mL/min/kg: rat= 55.2, dog= 30.9, human= 20.7, mouse= 90.

X-ray crystallography. Crystallographic methods and the production and use of the TMLR proteins were as previously described.[34]

ASSOCIATED CONTENT

Supporting Information. Kinase selectivity profiling data for **21**; X-ray structure of **21** complexed with EGFR TMLR double mutant (PDB code 5HCZ); crystallographic data collection and refinement statistics; molecular modeling methods; in vivo xenograft pharmacodynamics studies materials and methods; experimental details for the preparation of all compounds; NMR spectra for key compounds. This material is available free of charge via the Internet at http://pubs.acs.org.

Accession codes

PDB codes are the following: TMLR/**3**, 5CAS; TMLR/**7**, 5HCX; TMLR/**13**, 5HCY; TMLR/**21**, 5HCZ. Authors will release the atomic coordinates and experimental data upon article publication.

AUTHOR INFORMATION

Corresponding Author

*Email: chan.bryan@gene.com; Phone: 1-650-225-1000.

Author Contributions

The manuscript was written through contributions of all authors. All authors have given approval to the final version of the manuscript.

Notes

The authors declare no competing financial interest.

ACKNOWLEDGMENT

The authors thank Crystallographic Consulting LLC for diffraction data collection services and Mark Ultsch and Christine Huang for assistance with some crystals. The Advanced Light Source (ALS) is supported by the Director, Office of Science, Office of Basic Energy Sciences, of the U.S. Department of Energy under Contract No. DE-AC0205CH11231. The Berkeley Center for Structural Biology is supported in part by the National Institutes of Health, National Institute of General Medical Sciences, and the Howard Hughes Medical Institute. Use of the Stanford Synchrotron Radiation Lightsource (SSRL), SLAC National Accelerator Laboratory, is supported by the U.S. Department of Energy, Office of Science, Office of Basic Energy Sciences under Contract No. DE-AC02-76SF00515. The SSRL Structural Molecular Biology Program is

supported by the DOE Office of Biological and Environmental Research, and by the National Institutes of Health, National Institute of General Medical Sciences (including P41GM103393). The authors thank the analytical and purification groups at Genentech and Argenta for compound purification and characterization. The authors thank Savita Ubhayakar, Xiaorong Liang, Ning Liu, Quynh Ho, and Kirsten Messick for in vitro and in vivo PK and bioanalytical support. The authors also thank Professor François Diederich for the stimulating discussions.

ABBREVIATIONS

A, apical; Amphos, di-*tert*-butyl(4-dimethylaminophenyl)phosphine; ADME, absorption, distribution, metabolism, elimination; B, basolateral; BID, twice a day; BrettPhos, 2-(Dicyclohexylphosphino)3,6-dimethoxy-2′,4′,6′-triisopropyl-1,1′-biphenyl; Cl_{hep}, predicted hepatic clearance; $del_{746\text{-}750}$, epidermal growth factor receptor ($del_{746\text{-}750}$); DIEA, diisopropylethylamine; dppf, 1,1'-Bis(diphenylphosphino)ferrocene; EGFR, epidermal growth factor receptor; ER, erlotinib resistant; F_u, unbound fraction; H, human; HBTU, *N*,*N*,*N'*,*N'*-tetramethyl-*O*-(*1H*-benzotriazol-1-yl)uronium hexafluorophosphate; Hep, hepatocytes; K. sol, kinetic solubility; L858R, epidermal growth factor receptor (L858R); LM, liver microsomes; M, mouse; MCT, medium chain triglyerides; MDCK, Madin-Darby canine kidney; NSCLC, non-small cell lung cancer; P_{app}, apparent permeability; $Pd_2(dba)_3$, tris(dibenzylideneacetone)dipalladium(0); pEGFR, phosphorylated epidermal growth factor receptor; quant., quantitative; R, rat; TMLR, epidermal growth factor receptor (T790M/L858R); TMdel, epidermal growth factor receptor (T790M/$del_{746\text{-}750}$); TPSA, topological polar surface area; wtEGFR, wild type epidermal growth factor receptor; XPhos, 2-Dicyclohexylphosphino-2′,4′,6′-triisopropylbiphenyl; XantPhos, 4,5-Bis(diphenylphosphino)-9,9-dimethylxanthene.

REFERENCES

(1) Gazdar, A. F.; Minna, J. D. Inhibition of EGFR signaling: all mutations are not created equal. *PLoS Med.* **2005,** *2*, e377.

(2) Sharma, S. V.; Bell, D. W.; Settleman, J.; Haber, D. A. Epidermal growth factor receptor mutations in lung cancer. *Nat. Rev. Cancer* **2007,** *7*, 169-181.

(3) Sordella, R.; Bell, D. W.; Haber, D. A.; Settleman, J. Gefitinib-sensitizing EGFR mutations in lung cancer activate anti-apoptotic pathways. *Science* **2004,** *305*, 1163-1167.

(4) Tracy, S.; Mukohara, T.; Hansen, M.; Meyerson, M.; Johnson, B. E.; Janne, P. A. Gefitinib induces apoptosis in the EGFRL858R non-small-cell lung cancer cell line H3255. *Cancer Res.* **2004,** *64*, 7241-7244.

(5) Sharma, S. V.; Settleman, J. Oncogene addiction: setting the stage for molecularly targeted cancer therapy. *Gene. Dev.* **2007,** *21*, 3214-3231.

(6) Jackman, D. M.; Miller, V. A.; Cioffredi, L. A.; Yeap, B. Y.; Janne, P. A.; Riely, G. J.; Ruiz, M. G.; Giaccone, G.; Sequist, L. V.; Johnson, B. E. Impact of epidermal growth factor receptor and KRAS mutations on clinical outcomes in previously untreated non-small cell lung cancer patients: results of an online tumor registry of clinical trials. *Clin. Cancer Res.* **2009,** *15*, 5267-5273.

(7) Rosell, R.; Moran, T.; Queralt, C.; Porta, R.; Cardenal, F.; Camps, C.; Majem, M.; Lopez-Vivanco, G.; Isla, D.; Provencio, M.; Insa, A.; Massuti, B.; Gonzalez-Larriba, J. L.; Paz-Ares, L.; Bover, I.; Garcia-Campelo, R.; Moreno, M. A.; Catot, S.; Rolfo, C.; Reguart, N.; Palmero, R.; Sanchez, J. M.; Bastus, R.; Mayo, C.; Bertran-Alamillo, J.; Molina, M. A.; Sanchez, J. J.; Taron,

M. Screening for epidermal growth factor receptor mutations in lung cancer. *N. Engl. J. Med.* **2009,** *361*, 958-967.

(8) Lynch, T. J.; Bell, D. W.; Sordella, R.; Gurubhagavatula, S.; Okimoto, R. A.; Brannigan, B. W.; Harris, P. L.; Haserlat, S. M.; Supko, J. G.; Haluska, F. G.; Louis, D. N.; Christiani, D. C.; Settleman, J.; Haber, D. A. Activating mutations in the epidermal growth factor receptor underlying responsiveness of non-small-cell lung cancer to gefitinib. *N. Engl. J. Med.* **2004,** *350*, 2129-2139.

(9) Paez, J. G.; Janne, P. A.; Lee, J. C.; Tracy, S.; Greulich, H.; Gabriel, S.; Herman, P.; Kaye, F. J.; Lindeman, N.; Boggon, T. J.; Naoki, K.; Sasaki, H.; Fujii, Y.; Eck, M. J.; Sellers, W. R.; Johnson, B. E.; Meyerson, M. EGFR mutations in lung cancer: correlation with clinical response to gefitinib therapy. *Science* **2004,** *304*, 1497-1500.

(10) Pao, W.; Miller, V.; Zakowski, M.; Doherty, J.; Politi, K.; Sarkaria, I.; Singh, B.; Heelan, R.; Rusch, V.; Fulton, L.; Mardis, E.; Kupfer, D.; Wilson, R.; Kris, M.; Varmus, H. EGF receptor gene mutations are common in lung cancers from "never smokers" and are associated with sensitivity of tumors to gefitinib and erlotinib. *Proc. Natl. Acad. Sci. U. S. A.* **2004,** *101*, 13306-13311.

(11) Janne, P. A.; Schellens, J. H.; Engelman, J. A.; Eckhardt, S. G.; Millham, R.; Denis, L. J.; Britten, C. D.; Wong, S. G.; Boss, D. S.; Camidge, D. R. Preliminary activity and safety results from a phase I clinical trial of PF-00299804, an irreversible pan-HER inhibitor, in patients (pts) with NSCLC. *J. Clin. Oncol.* **2008,** *26*, (May 20 suppl; abstr 8027).

(12) Sequist, L. V.; Besse, B.; Lynch, T. J.; Miller, V. A.; Wong, K. K.; Gitlitz, B.; Eaton, K.; Zacharchuk, C.; Freyman, A.; Powell, C.; Ananthakrishnan, R.; Quinn, S.; Soria, J. C. Neratinib,

an irreversible pan-ErbB receptor tyrosine kinase inhibitor: results of a phase II trial in patients with advanced non-small-cell lung cancer. *J Clin. Oncol.* **2010,** *28*, 3076-3083.

(13) Pao, W.; Chmielecki, J. Rational, biologically based treatment of EGFR-mutant non-small-cell lung cancer. *Nat. Rev. Cancer* **2010,** *10*, 760-774.

(14) Kobayashi, S.; Boggon, T. J.; Dayaram, T.; Janne, P. A.; Kocher, O.; Meyerson, M.; Johnson, B. E.; Eck, M. J.; Tenen, D. G.; Halmos, B. EGFR mutation and resistance of non-small-cell lung cancer to gefitinib. *N. Engl. J. Med.* **2005,** *352*, 786-792.

(15) Pao, W.; Miller, V. A.; Politi, K. A.; Riely, G. J.; Somwar, R.; Zakowski, M. F.; Kris, M. G.; Varmus, H. Acquired resistance of lung adenocarcinomas to gefitinib or erlotinib is associated with a second mutation in the EGFR kinase domain. *PLoS Med.* **2005,** *2*, e73.

(16) Engel, J.; Lategahn, J.; Rauh, D. Hope and Disappointment: Covalent Inhibitors to Overcome Drug Resistance in Non-Small Cell Lung Cancer. *ACS Med. Chem. Lett.* **2016**, *7*, 2-5.

(17) Yu, H. A.; Arcila, M. E.; Rekhtman, N.; Sima, C. S.; Zakowski, M. F.; Pao, W.; Kris, M. G.; Miller, V. A.; Ladanyi, M.; Riely, G. J. Analysis of tumor specimens at the time of acquired resistance to EGFR-TKI therapy in 155 patients with EGFR-mutant lung cancers. *Clin. Cancer Res.* **2013,** *19*, 2240-2247.

(18) Kosaka, T.; Yatabe, Y.; Endoh, H.; Yoshida, K.; Hida, T.; Tsuboi, M.; Tada, H.; Kuwano, H.; Mitsudomi, T. Analysis of epidermal growth factor receptor gene mutation in patients with non-small cell lung cancer and acquired resistance to gefitinib. *Clin. Cancer Res.* **2006,** *12*, 5764-5769.

(19) Balak, M. N.; Gong, Y.; Riely, G. J.; Somwar, R.; Li, A. R.; Zakowski, M. F.; Chiang, A.; Yang, G.; Ouerfelli, O.; Kris, M. G.; Ladanyi, M.; Miller, V. A.; Pao, W. Novel D761Y and common secondary T790M mutations in epidermal growth factor receptor-mutant lung adenocarcinomas with acquired resistance to kinase inhibitors. *Clin. Cancer Res.* **2006,** *12*, 6494-6501.

(20) Erlotinib activity in biochemical assays: wtEGFR Ki = 0.1 nM, EGFR($del_{746-750}$) Ki = 0.1 nM, EGFR(T790M/L858R) Ki = 123 nM, EGFR(T790M/$del_{746-750}$) Ki = 95 nM.

(21) Kwak, E. L.; Sordella, R.; Bell, D. W.; Godin-Heymann, N.; Okimoto, R. A.; Brannigan, B. W.; Harris, P. L.; Driscoll, D. R.; Fidias, P.; Lynch, T. J.; Rabindran, S. K.; McGinnis, J. P.; Wissner, A.; Sharma, S. V.; Isselbacher, K. J.; Settleman, J.; Haber, D. A. Irreversible inhibitors of the EGF receptor may circumvent acquired resistance to gefitinib. *Proc. Natl. Acad. Sci. U. S. A.* **2005,** *102*, 7665-7670.

(22) Shah, N. P.; Nicoll, J. M.; Nagar, B.; Gorre, M. E.; Paquette, R. L.; Kuriyan, J.; Sawyers, C. L. Multiple BCR-ABL kinase domain mutations confer polyclonal resistance to the tyrosine kinase inhibitor imatinib (STI571) in chronic phase and blast crisis chronic myeloid leukemia. *Cancer Cell* **2002,** *2*, 117-125.

(23) Quintas-Cardama, A.; Kantarjian, H.; Cortes, J. Flying under the radar: the new wave of BCR-ABL inhibitors. *Nat. Rev. Drug Discov.* **2007,** *6*, 834-848.

(24) Yun, C. H.; Mengwasser, K. E.; Toms, A. V.; Woo, M. S.; Greulich, H.; Wong, K. K.; Meyerson, M.; Eck, M. J. The T790M mutation in EGFR kinase causes drug resistance by increasing the affinity for ATP. *Proc. Natl. Acad. Sci. U. S. A.* **2008,** *105*, 2070-2075.

(25) Soria, J.-C.; Sequist, L. V.; Gadgeel, S.; Goldman, J.; Wakelee, H.; Varga, A.; Fidias, P.; Wozniak, A. J.; Neal, J. W.; Doebele, R. C.; Garon, E. B.; Jaw-Tsai, S.; Caunt, L.; Kaur, P.; Rolfe, L.; Allen, A.; Camidge, D. R. First-in-human evaluation of CO-1686, an irreversible, highly selective tyrosine kinase inhibitor of mutations of EGFR (activating and T790M). In *15th World Conference on Lung Cancer*, Sydney, Australia, 2013.

(26) Ranson, M. Preliminary results from a Phase I study with AZD9291. In *European Cancer Congress*, 2013.

(27) Cross, D. A. E.; Ashton, S. E.; Ghiorghiu, S.; Eberlein, C.; Nebhan, C. A.; Spitzler, P. J.; Orme, J. P.; Finlay, M. R. V.; Ward, R. A.; Mellor, M. J.; Hughes, G.; Rahi, A.; Jacobs, V. N.; Brewer, M. R.; Ichihara, E.; Sun, J.; Jin, H.; Ballard, P.; Al-Kadhimi, K.; Rowlinson, R.; Klinowska, T.; Richmond, G. H. P.; Cantarini, M.; Kim, D.-W.; Ranson, M. R.; Pao, W. AZD9291, an Irreversible EGFR TKI, Overcomes T790M-Mediated Resistance to EGFR Inhibitors in Lung Cancer. *Cancer Discov.* **2014,** *4*, 1046-1061.

(28) Sjin, R. T. T.; Lee, K.; Walter, A. O.; Dubrovskiy, A.; Sheets, M.; Martin, T. S.; Labenski, M. T.; Zhu, Z.; Tester, R.; Karp, R.; Medikonda, A.; Chaturvedi, P.; Ren, Y.; Haringsma, H.; Etter, J.; Raponi, M.; Simmons, A. D.; Harding, T. C.; Niu, D.; Nacht, M.; Westlin, W. F.; Petter, R. C.; Allen, A.; Singh, J. In Vitro and In Vivo Characterization of Irreversible Mutant-Selective EGFR Inhibitors That Are Wild-Type Sparing. *Mol. Cancer Ther.* **2014,** *13*, 1-12.

(29) Janne, P. A.; Ramaligam, S. S.; Yang, J. C. H.; Ahn, M.-J.; Kim, D.-W.; Kim, S.-W.; Planchard, D.; Ohe, Y.; Felip, E.; Watkins, C.; Cantarini, M.; Ghiorghiu, S.; Ranson, M. Clinical activity of the mutant-selective EGFR inhibitor AZD9291 in patients (pts) with EGFR inhibitor-resistant non-small-cell lung cancer (NSCLC). *J. Clin. Oncol.* **2014,** *32*, 8009.

(30) Jänne, P. A.; Yang, J. C.-H.; Kim, D.-W.; Planchard, D.; Ohe, Y.; Ramalingam, S. S.; Ahn, M.-J.; Kim, S.-W.; Su, W.-C.; Horn, L.; Haggstrom, D.; Felip, E.; Kim, J.-H.; Frewer, P.; Cantarini, M.; Brown, K. H.; Dickinson, P. A.; Ghiorghiu, S.; Ranson, M. AZD9291 in EGFR Inhibitor Resistant Non Small-Cell Lung Cancer. *N. Engl. J. Med.* **2015,** *372*, 1689-1699.

(31) Thress, K. S.; Paweletz, C. P.; Felip, E.; Cho, B. C.; Stetson, D.; Dougherty, B.; Lai, Z.; Markovets, A.; Vivancos, A.; Kuang, Y.; Ercan, D.; Matthews, S. E.; Cantarini, M.; Barrett, J. C.; Janne, P. A.; Oxnard, G. R. Acquired EGFR C797S mutation mediates resistance to AZD9291 in non-small cell lung cancer harboring EGFR T790M. *Nat. Med.* **2015**, *21*, 560-562.

(32) Yu, H. A.; Tian, S. K.; Drilon, A. E.; Borsu, L.; Riely, G. J.; Arcila, M. E.; Ladanyi, M. Acquired Resistance of EGFR-Mutant Lung Cancer to a T790M-Specific EGFR Inhibitor: Emergence of a Third Mutation (C797S) in the EGFR Tyrosine Kinase Domain. *JAMA Oncology* **2015,** *7*, 982-984.

(33) Song, Z.; Ge, Y; Wang, C.; Huang, S.; Shu, X.; Liu, K.; Zhou, Y.; Ma, X. Challenges and Perspectives on the Development of Small-Molecule EGFR Inhibitors against T790M-Mediated Resistance in Non-Small Cell Lung Cancer. *J. Med. Chem.* **2016**, *59*, 6580-6594.

(34) Heald, R. A.; Chan. B. K.; Bryan, M. C.; Eigenbrot, C.; Yu, C.; Burdick, D.; Hanan, E. J.; Chan, E.; Schaefer, G.; La, H.; Purkey, H.; Knight, J.; Yen, I.; Jackson, P.; Bowman, K.; Mortara, K.; Lainchbury, M.; Shao, L.; Elliott, R.; Seward, E.; Malek, S.; Schmidt, S.; Sideris, S.; Heffron, T. P.; Yeap, K.; Chen, Y.; Mann, S.; Noncovalent Mutant Selective Epidermal Growth Factor Receptor Inhibitors: A Lead Optimization Case History. *J. Med. Chem.* **2015**, *58*, 8877-8895.

(35) Hanan, E. J.; Eigenbrot, C.; Bryan, M. C.; Burdick, D. J.; Chan, B. K.; Chen, Y.; Dotson, J.; Heald, R. A.; Jackson, P. S.; La, H.; Lainchbury, M. D.; Malek, S.; Purkey, H. E.; Schaefer G.; Schmidt. S.; Seward, E. M.; Sideris, S.; Tam, C.; Wang, S.; Yeap, S. K.; Yen, I.; Yin, J.; Yu, C.; Zilberleyb, I.; Heffron, T. P. Discovery of Selective and Noncovalent Diaminopyrimidine-Based Inhibitors of Epidermal Growth Factor Receptor Containing the T790M Resistance Mutation. *J. Med. Chem.* **2014**, *57*, 10176-10191.

(36) Oxnard, G. R.; Janjigian, Y. Y.; Arcila, M. E.; Sima, C. S.; Kass, S. L.; Riely, G. J.; Pao, W.; Kris, M. G.; Ladanyl, M.; Azzoli, C. G.; Miller, V. A. Maintained Sensitivity to EGFR Tyrosine Kinase Inhibitors in EGFR-Mutant Lung Cancer Recurring after Adjuvant Erlotinib or *Gefitinib. Clin. Cancer Res*. **2011**, *19*, 6322-6328.

(37) Lipinski, C. A.; Lombardo, F., Dominy, B. W.; Feeney, P. J. Experimental and computational approaches to estimate solubility and permeability in drug discovery and development settings. *Adv. Drug Delivery Rev*. **1997**, *23*, 3-25.

(38) Ritchie, T. J.; Macdonald, S. J. F.; Young, R. J.; Pickett, S. D. The impact of aromatic ring count on compound developability: Further insights by examining carbo- and hetero-aromatic and aliphatic ring types. *Drug Discov. Today* **2011**, *16*, 164-171.

(39) Halladay, J. S.; Wong, S.; Jaffer, S. M.; Sinhababu, A. K.; Khojasteh-Bakht, S. C. Metabolic Stability Screen for Drug Discovery Using Cassette Analysis and Column Switching. *Drug Metab. Lett.* **2014**, *1*, 67-72.

(40) Obach, R. S.; Baxter, J. G.; Liston, T. E.; Silber, B. M.; Jones, B. C.; MacIntyre, F.; Rance, D. J.; Wastall, P. *J. Pharmacol. Exp. Ther.* **1997**, *283*, 46-58.

Table of Contents Graphic

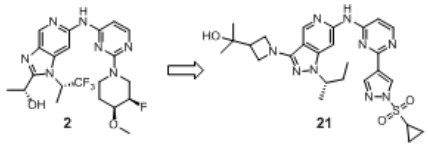

Cell line	Mutant Status	2	21
H1975 pEGFR IC_{50} (μM)	T790M-L858R	0.261	0.027
PC9-ER pEGFR IC_{50} (μM)	T790M-$del_{746-750}$	0.081	0.009
PC9 pEGFR IC_{50} (μM)	$del_{746-750}$	5.4	0.033
H292 pEGFR IC_{50} (μM)	wildtype	>10	0.218